Reprinted From
THEORETICAL CHEMISTRY: Advances and Perspectives VOL. 3

Academic Press, Inc.
New York San Francisco London

Proton Transfer Reactions and Kinetics in Water

Frank H. Stillinger
Bell Laboratories
Murray Hill, New Jersey

I. Introduction and Survey

A. Molecular Nature of Pure Water

Undoubtedly the most important solvent in chemistry and chemical technology is water. Furthermore, this substance plays an active and indispensable role in biology. Chemical reactions that take place in water exhibit enormous diversity and frequently possess great industrial, geological, and medical significance. Under these circumstances, then, it is natural to devote serious attention to specific study of chemical reactions in water at the molecular level.

Among all possible chemical reactions that occur in water, the most fundamental is the reversible dissociation reaction

$$H_2O \underset{k_a}{\overset{k_d}{\rightleftharpoons}} H^+ + OH^-. \tag{1.1}$$

Examination of the theory describing forward and reverse rates, and of the nature of the solvated ions formed, constitutes a major objective in this chapter. In addition, we shall broaden the scope to include other aqueous-medium reactions involving proton transfer.

Basic to the understanding of proton transfer reactions and kinetics in water is an understanding of the molecular nature of water itself. Both experimental and theoretical research on water has recently been intense, and as a result of those activities a reasonably complete picture has begun to emerge (Stillinger, 1975, 1977).

In large measure, the structure and properties of water can be explained by the shape of the individual molecules, and by the tendency of those molecules to hydrogen bond to one another. The ground state of the isolated water molecule displays C_{2v} symmetry; the OH bond lengths are 0.9576 Å, and form angle 104.48° at the oxygen nucleus (Benedict *et al.*, 1956). The hydrogen bonds that hold together the condensed phases of water are in undistorted form essentially linear, with an OH covalent bond of one molecule (the proton donor) pointing toward the back side of a neighbor molecule's oxygen atom (the proton acceptor). Participant molecules in a hydrogen bond normally are little distorted from their isolated geometries. Well-formed hydrogen bonds between water molecules have oxygen–oxygen lengths in the range 2.7–3.0 Å, and strength about 5 kcal/mole (Hankins *et al.*, 1970; Popkie *et al.*, 1973).

Hydrogen bonding between neighboring water molecules achieves its greatest extent in the crystal structure of ordinary hexagonal ice (Fletcher, 1970). There, each molecule participates in precisely four hydrogen bonds to nearest neighbors 2.76 Å away. Toward two of these neighbors the central molecule acts as proton donor, while from the other two it accepts protons. The spatial arrangement of these four bonds is the same as four lines radiat-

ing outward from the center of a regular tetrahedron toward its vertices. The existence of this tetrahedral coordination with 109.45° between successive bonds is doubtless encouraged by the fact that the isolated-molecule HOH angle is close to that ideally required for strictly linear hydrogen bonds in the crystal.

The hydrogen bonds in hexagonal ice form a space-filling network in which the bonds are locally arranged in hexagons. These hexagons exist in both "chair" and "boat" conformations, analogous to those adopted by the hydrocarbon cyclohexane (Wiberg, 1964). The low temperature cubic modification of ice is similar, but contains only chair hexagons.

The propensity for water molecules to retain tetrahedral coordination through hydrogen bonds to neighbors, with modest angular deformation, is obvious from examination of the structures of the high pressure ices II–IX (Fletcher, 1970). In each case, space-filling networks of hydrogen bonds exist, but the polygons locally produced include quadrilaterals, pentagons, hexagons, and octagons. Even this rich geometric diversity is further broadened by consideration of water networks in clathrate hydrates; in the case of *tert*-butylamine hydrate the unit cell contains a heptagon of hydrogen bonds (Jeffrey *et al.*, 1967).

Evidently the tendency for water to engage in tetrahedral hydrogen bonding extends beyond the melting point of ice into liquid water. X-Ray and neutron diffraction studies of the liquid strongly suggest this qualitative behavior, but with a significant degree of disruption (Narten, 1972). As would be expected, increasing temperature measurably increases the extent of that disruption (Narten and Levy, 1971).

Computer simulation studies have recently been carried out for liquid water. They include both the Monte Carlo (Lie and Clementi, 1975) and molecular dynamics (Stillinger and Rahman, 1974) techniques. These simulations provide confirmation for conclusions drawn from the diffraction experiments about local tetrahedral order in the liquid. They also provide a wealth of additional geometric information about molecular order and hydrogen bond arrangements that is unavailable from any conceivable experiment (Rahman and Stillinger, 1973).

The conclusion that can be drawn from experimental and theoretical studies is that liquid water consists of a random hydrogen bond network, including strained and broken bonds. Furthermore, hydrogen-bond polygons of all sizes larger than triangles are present, with no marked preference for even or for odd numbers of sides (Rahman and Stillinger, 1973). This random network is labile, with bonds breaking and reforming nearby so as to permit diffusion and fluid flow. There is no compelling evidence to suggest that the random network is broken up into patches or regions unconnected to the remainder, but instead a rather uniform degree of hydrogen bond connectivity obtains throughout.

Compared to most other liquids, water has a high static dielectric constant ε_0. At atmospheric pressure, ε_0 is 87.74 at 0°C, but drops to 55.72 at 100°C (Malmberg and Maryott, 1956). To a large degree these high values reflect the polar nature of the water molecule, which in isolation possesses static dipole moment

$$\mu = 1.855 \times 10^{-18} \text{ esu cm} \tag{1.2}$$

(Dyke and Muenter, 1973). It is a simple matter to show that *locally uncorrelated* dipoles would alone produce a static dielectric constant determined by the formula

$$\frac{(\varepsilon_0 - 1)(2\varepsilon_0 + 1)}{\varepsilon_0} = \frac{4\pi\rho\mu^2}{k_B T}, \tag{1.3}$$

where ρ is the molecular number density, k_B is Boltzmann's constant, and T is the absolute temperature. By inserting the μ value shown in Eq. (1.2), and the appropriate ρ values, one finds that Eq. (1.3) predicts

$$\begin{aligned} \varepsilon_0 &= 19.70 \quad (0°\text{C}), \\ &= 13.98 \quad (100°\text{C}). \end{aligned} \tag{1.4}$$

That the measured ε_0 values are substantially larger stems from the failure of naive formula (1.3) to incorporate three important phenomena.

1. The molecules can polarize in an externally applied electric field, due to both nuclear deformation and polarization of the electronic distribution.
2. Even in the absence of an external field, interactions between neighbor molecules in the random network tend on the average to increase the molecular dipole moment to a value $\bar{\mu}$ substantially exceeding μ.
3. Nearby pairs of molecules tend to have their dipole directions biased toward parallelism. The total local moment near a given molecule is frequently denoted by $g_K \bar{\boldsymbol{\mu}}$, where g_K is the Kirkwood orientational correlation factor (Kirkwood, 1939).

Unfortunately there is no fully satisfactory theory for ε_0 in water that accounts for all of these effects quantitatively. Nevertheless, rough estimates both for $\bar{\mu}$ and for g_K have often been proposed (Eisenberg and Kauzmann, 1969) with

$$\begin{aligned} g_K &\approx 2.6, \\ \bar{\mu} &\approx 2.4 \times 10^{-18} \text{ esu cm} \end{aligned} \tag{1.5}$$

for water around room temperature, and with both quantities exhibiting negative temperature coefficients.

The rate at which the random hydrogen-bond network in water spontaneously restructures itself can be monitored by measurements of self-diffusion

constants (Mills, 1973), viscosity (Stokes and Mills, 1965), and dielectric relaxation times (Collie *et al.*, 1948). Each of these exhibits strong temperature dependence. The respective Arrhenius plots are distinctly curved, with inferred energies of activation increasing as T declines (Eisenberg and Kauzmann, 1969). These increases are particularly noticeable if data for supercooled water are included, and they surely reflect the energy required for thermal disruption of the random hydrogen-bond network. It is interesting to note in this regard that as water at 0°C freezes to hexagonal ice, the self-diffusion constant decreases discontinuously by a factor of about 10^{-5}, while the dielectric relaxation time increases by about 10^6.

Even without further knowledge, one would reasonably expect other rate processes in water, involving proton transfer, to display similar temperature effects. We will see how that expectation is in fact realized.

B. Dissociation and Electrical Conduction Measurements

The conventional definition of pH for a solution containing H^+ ions is

$$\mathrm{pH} = -\log_{10} a_{H^+}, \tag{1.6}$$

where a_{H^+} is the activity of those ions referred to the hypothetical standard state of unit molar concentration in pure water. Of course, single ion activities are unmeasurable by the normal procedures of solution physical chemistry, so evaluation of pH would seem to require auxilliary assumptions or theoretical calculations.

Under ordinary temperature and pressure conditions, the extent of dissociation in pure water is sufficiently small that the resulting solution of H^+ and OH^- ions is essentially ideal. In that case a_{H^+} in Eq. (1.6) may validly be replaced by the molar concentration of H^+ ions, C_{H^+}. Under other conditions leading to high degree of dissociation, or if concentrated solutes are present, this replacement is unjustified.

The dissociation constant for water K_w is given by the ratio of rate constants in Eq. (1.1):

$$\begin{aligned} K_w &= k_d/k_a \\ &= a_{H^+} a_{OH^-}/a_{H_2O}, \end{aligned} \tag{1.7}$$

where of course in the last form shown a consistent set of standard states must be used for the activities a_i. A closely related constant K'_w can be measured electrochemically, by observing emf's for cells without liquid junctions. Specifically

$$K'_w = a_{H^+} a_{OH^-}/a'_{H_2O}, \tag{1.8}$$

where a_{H^+} and a_{OH^-} refer to the hypothetical 1 M standard state, and where

a'_{H_2O} refers to the standard state of pure water ($\approx$ 55.5 moles/liter). In view of the small extent of dissociation under the usual conditions, K'_w undergoes an important simplification to

$$K'_w = (C_{H^+})^2, \tag{1.9}$$

from which pH may then be determined.

In the temperature range 0°–60°C, values determined electrochemically for K'_w have been listed by Robinson and Stokes (1959). These results are well represented by the formula

$$-\log_{10} K'_w = \frac{4471.33}{T} - 6.0846 + 0.017053T. \tag{1.10}$$

Table I reports concentrations of H^+ and OH^- ions produced by dissociation in pure water that have been determined through K'_w.

Table I

ION CONCENTRATIONS RESULTING FROM DISSOCIATION OF PURE WATER AT VARIOUS TEMPERATURES[a]

t(°C)	$C_{H^+}=C_{OH^-}$ (10^{-7} moles/l)
0	0.337
5	0.430
10	0.540
15	0.671
20	0.825
25	1.004
30	1.212
35	1.445
40	1.708
45	2.004
50	2.340
55	2.701
60	3.101

[a] From Robinson and Stokes (1959).

By differentiating $\log_{10} K'_w$ with respect to temperature, standard thermodynamic changes in enthalpy, entropy, and heat capacity may be determined for the dissociation process. The currently preferred values at 298°K for these quantities, respectively, are the following (Hepler and Woolley, 1973):

$$\begin{aligned} \Delta H^0 &= 13.34 \text{ kcal/mole}, \\ \Delta S^0 &= -19.31 \text{ cal/mole deg}, \\ \Delta C_p^0 &= -53.5 \text{ cal/mole deg}. \end{aligned} \tag{1.11}$$

The standard-state volume change for the reaction can either be determined from pressure variation of K'_w, or from dilatometric measurements of dilute acid–base neutralizations. The preferred value at 298°K is (Hepler and Wooley, 1973)

$$\Delta V^0 = -22.13 \text{ cm}^3/\text{mole}. \tag{1.12}$$

This result quantitatively summarizes the tendency for increasing pressure to shift equilibrium in Eq. (1.1) toward greater dissociation (Hamann, 1963). It also suggests that significant electrostriction occurs around the solvated H^+ and OH^- ions, although the manner in which the random hydrogen-bond network reorganizes to accommodate that electrostriction must be determined by other means.

The galvanic cell method is not useful for study of dissociation in water under extreme temperature and pressure conditions. Instead, K'_w and the ionic concentrations may be obtained from the specific conductance and the limiting equivalent conductance of water. Tödheide (1972) reviews the present status of these measurements and their implications. It is interesting to note that K'_w reaches 10^{-2} at about 1000°C and 100 kbar, with no diminution of the trend toward even greater dissociation as T and p continue to rise. Indeed a very recent report (Vereschagin, *et al.*, 1975) seems to indicate that pressure of about 1 Mbar may suffice to produce nearly complete ionic dissociation.

The limiting equivalent conductances $\lambda^0_{H^+}$ and $\lambda^0_{OH^-}$ are far larger than the same quantities for any other ions. Table II provides values in the range 0°–100°C, at 1 atm. Included for comparison are results for Na^+ and Cl^- in water, which can be regarded as "typical" monovalent ions.

Table II

LIMITING EQUIVALENT CONDUCTANCES FOR IONS IN WATER[a,b]

t(°C)	$\lambda^\circ_{H^+}$	$\lambda^\circ_{OH^-}$	$\lambda^\circ_{Na^+}$	$\lambda^\circ_{Cl^-}$	$\eta\lambda^\circ_{H^+}$	$\eta\lambda^\circ_{OH^-}$	$\eta\lambda^\circ_{Na^+}$	$\eta\lambda^\circ_{Cl^-}$
0	225	105	26.5	41.0	402	188	47.4	73.3
5	250.1		30.3	47.5	379		45.9	72.0
15	300.6	165.9	39.7	61.4	342	189	45.1	69.8
18	315	175.8	42.8	66.0	332	185	45.1	69.5
25	349.8	199.1	50.10	76.35	311	177	44.6	68.0
35	397.0	233.0	61.5	92.2	286	168	44.2	66.3
45	441.4	267.2	73.7	108.9	263	159	43.9	64.9
55	483.1	301.4	86.8	126.4	243	152	43.7	63.7
100	630	450	145	212	178	127	41.0	60.0

[a] From Robinson and Stokes (1959), p. 465.
[b] λ^0_i in cm²/ohm equiv., η in centipoise.

For ions that move as spheres in a structureless, viscous solvent, the product $\lambda_i^0 \eta$ should be constant (η = solvent viscosity). Table II shows this is not quite the case even for "typical" ions. Instead, the product declines somewhat with rising temperature. However, the corresponding decline is significantly greater for OH^- and quite dramatic indeed for H^+. Once again H^+ and OH^- act anomalously.

The explanation offered years ago by Bernal and Fowler (1933) (following Grottius and Hückel) for the anomalous mobilities of H^+ and OH^- is still regarded as essentially correct. It rests upon the existence of connected

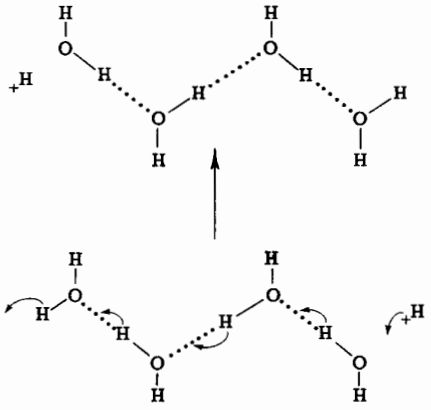

Fig. 1. Electrical conduction of protons in water, by successive hydrogen shifts along a chain of hydrogen bonds.

hydrogen-bond pathways within water and is relevant both to ice and to the liquid. An excess proton at one end of a chain of hydrogen bonds can cause a sequence of proton shifts, each along its own hydrogen bond, whose net result amounts to transfer of the excess proton to the other end of the chain. Similarly, a chain of hydrogen bonds terminating at OH^- (a "missing" proton, or proton "hole") can effectively cause transfer of that ion to its other end by proton shifts in the opposite direction. Figure 1 schematically illustrates the first, and Fig. 2 the second, of these sequential shifts.

Although present knowledge of H^+ and OH^- mobilities in ice is rather imprecise, it appears that freezing water causes both ions to move with greater difficulty. Presently available results for ice (Onsager, 1973) suggest that the H^+ mobility discontinuously drops by a factor of about two, and that of OH^- by roughly a factor of ten, as a result of freezing. At first this seems paradoxical, since hydrogen bond chains are obviously more perfect and more extended in ice than in the liquid. However, one must realize that the rigid ice lattice is largely inconsistent with the negative volume change

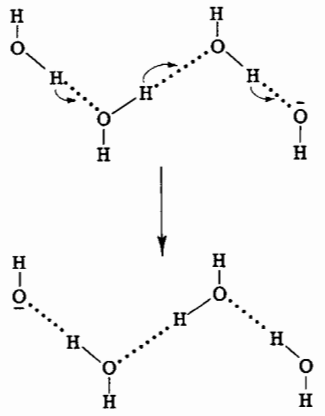

Fig. 2. Mechanism for hydroxide anion mobility in water. The proton "hole" moves by successive hydrogen shifts akin to those shown in Fig. 1.

that normally accompanies dissociation in the liquid. Consequently, the structure around H^+ and OH^- in ice should differ significantly from the corresponding liquid structure, in particular as regards hydrogen-bond lengths. The constraints imposed by the surrounding ice crystal thus appear to retard ionic mobility.

The structural studies of hydrated H^+ and OH^- covered in Sections II,B and C below support this conclusion in a general way, and suggest new details of the ionic transport process. In particular, the thermally induced rate of hydrogen-bond network restructuring must play a fundamental role in explaining the increase in H^+ and OH^- mobilities in the liquid as temperature rises.

C. Isotope Effects

Substitution of deuterium (D) or tritium (T) for hydrogen in water causes important chemical and physical changes. These changes encompass both equilibrium and kinetic properties. Table III provides comparisons between H_2O, D_2O, and T_2O for a short list of properties.

The increase shown in Table III for triple point temperature T_t and maximum-density temperature T_m, as hydrogen isotopic mass increases, clearly indicates an increasing hydrogen bond strength. The same bond-strength phenomenon is also illustrated by decrease in vapor pressure at 20°C, with hydrogen mass increase. However, note that the temperature shifts for T_t are proportionally different than those for T_m, so that the "law of corresponding states" does not apply. Consequently, the isotope effects are more complex than could be explained by mere change in potential energy

Table III

COMPARISON OF PROPERTIES FOR ISOTOPICALLY SUBSTITUTED WATERS

Property	H_2O	D_2O	T_2O
Triple point temperature, T_t(°C)	0.01[a]	3.83[a]	4.49[b]
Maximum-density temperature, T_m(°C)	3.98[a]	11.19[a]	13.40[a]
Critical temperature, T_c(°C)	374.15[a]	370.9[a]	
Static dielectric constant, ε_0 (at 20°C)	80.20[c]	79.89[c]	
Dielectric relaxation time, τ_d (psec, at 20°C)	9.55[a]	12.3[a]	
Self-diffusion constant, D (10^{-5} cm^2/sec, at 25°C)	2.299[d]	1.872[d]	
Dissociation constant, K'_w (10^{-14} moles^2/l^2, at 20°C)	0.681[e]	0.135[f]	
Shear viscosity, η (centipoise, at 30°C)	0.7975[a]	0.969[a]	
Vapor pressure (torr at 20°C)	17.535[g]	15.100[h]	14.553[h]
Second virial coefficient, B (cm^3/mole, at 250°C)	−159.6[i]	−160.7[i]	
Hydrogen ion limiting equivalent conductance, λ_i^0 (cm^2/ohm equiv., at 25°)	349.8[e]	242.4[j]	

[a] Eisenberg and Kauzmann (1969).
[b] Jones (1952).
[c] Vidulich *et al.* (1967).
[d] Mills (1973).
[e] Robinson and Stokes (1959).
[f] Covington *et al.* (1966).
[g] Weast (1975).
[h] Jones (1968).
[i] Kell *et al.* (1968).
[j] Kotowski (1964).

coupling strengths in an otherwise classical statistical mechanical description. Indeed, the critical temperatures T_c (at which most hydrogen bonds may be broken) exhibit a reversed trend.

Quantum-mechanical zero-point motion in water-molecule vibrational modes is important at room temperature owing to the small masses of hydrogen isotopes. Similarly, there are significant quantum effects in rotational motion. The observed differences in thermodynamic properties of H_2O, D_2O, and T_2O stem from the differing extent to which quantum corrections to classical vibration and (hindered) rotation apply to these substances.

The influences of vibrational and rotational quantum corrections to hydrogen bond strength are opposite. For the high-frequency OH stretch

modes in water, hydrogen bonding causes a decrease in frequency (Eisenberg and Kauzmann, 1969). The resulting energy reduction upon formation of a hydrogen bond is greater for H than for D, and least for T. Thus if only these stretch-mode vibrational zero-point shifts were at issue, H_2O would tend to have stronger hydrogen bonds than D_2O, and those in T_2O would be weakest of all. The symmetrical bend mode probably shifts in the opposite direction upon bonding (to higher frequency), but it bears relatively little zero-point energy, since it is much the lowest frequency of the three normal modes and so will exert relatively little influence.

Formation of hydrogen bonds turns free rotational motion into librational motion. In ice Ih formed from H_2O these librations fall in the frequency range around 840 cm^{-1} (Eisenberg and Kauzmann, 1969). Conversion of rotation to libration confines angular motion considerably, and must be accompanied by substantial zero-point motion which will *destabilize* the bonded structure. This bond destabilization evidently must be more influential the lighter the hydrogen isotope involved.

In view of the experimental observations, it is clear that librational and bend-mode destabilizations more than compensate for stretch-mode stabilization effects on hydrogen bonding at room temperature.

All rate processes slow down in pure water as hydrogen isotopic mass increases. For the most part these changes are larger in magnitude than those observed for static thermodynamic properties (although K'_w provides an obvious exception). In subsequent sections we shall seek a description of H^+ and OH^- solvation and kinetics which is fully consistent with these facts.

D. Chemical Reactions Involving Proton Transfer

The number of known chemical reactions that involve proton transfer is vast. An exhaustive survey of these reactions would be inappropriate for this article. Instead, it will suffice to illustrate the major classes of proton transfer reactions in water with a few concrete examples, indicating relevant experimental techniques along the way.

The fundamental reaction (1.1) for water itself is known to be characterized by an extremely high association rate constant k_a. Special relaxation methods are required to study such high rates; Eigen and DeMaeyer (1958) employed a rapid electrical pulse technique to study the dissociation field effect (Wien effect for weak electrolytes). They calculated that

$$k_a = (1.4 \pm 0.2) \times 10^{11} \text{ l/mole sec} \tag{1.13}$$

at 25°C. As they themselves stress, this result implies that a sudden mixture of 1 M solutions of strong base and strong acid would be followed by substantially complete neutralization within 10^{-11} sec or so. This extreme

speed is consistent only with diffusion-limited rates, i.e., the excess H^+ and OH^- particles need only to find each other to react. No transition state or obvious barrier to reaction exists.

By combining the k_a and K'_w values through Eq. (1.7) (along with the assumption $a_{H_2O} \approx 55.5$ moles/liter), one concludes that

$$k_d = 2.5 \times 10^{-5}/\text{sec} \tag{1.14}$$

at 25°C. This implies that a given intact water molecule will on the average take about 11 hours to dissociate spontaneously.

The strong electric fields that exist in the neighborhood of inorganic ions can severely perturb the dissociation equilibrium of neighboring water molecules. An extreme example is provided by the forced ionization of water molecules comprising the first shell of solvent molecules around an ion. A suitable example would be hydrolysis of the solvated ferric ion:

$$Fe(H_2O)_n^{3+} \rightleftharpoons Fe(H_2O)_{n-1}(OH)^{2+} + H^+. \tag{1.15}$$

It is obvious here that the high positive charge on Fe^{3+} encourages the proton to leave the vicinity, thus effectively reducing the local cationic charge by one unit. The extent of such hydrolysis reactions can be studied effectively by measuring the pH of dilute solutions of the metal salts of interest.

Dissociation of weak acids in water is analogous to reaction (1.1). The homologous series of carboxylic acids (formic, acetic, propionic, butyric, ...) offers a classical family of examples:

$$R - COOH \rightleftharpoons R - COO^- + H^+, \tag{1.16}$$

whose dissociation constants (acidity constants)

$$K_a = \frac{[RCOO^-][H^+]}{[RCOOH]} \tag{1.17}$$

can be determined by any convenient pH measurement technique in dilute solution. Members of this series are all stronger acids than water by far, with K_a values clustering around 1.5×10^{-5} mole/liter at 25°C (Fieser and Fieser, 1956) as the organic R-group increases in size. Changes in acidity upon substitution in the alkane chains is an important phenomenon whose explanation resides primarily in modification of the chemical nature of the dissociating molecule itself, rather than in perturbation of the surrounding solvent. As an example, we cite the case of the successively fluorinated acetic acids at 25°C (Chambers, 1973):

$$\begin{aligned} CH_3COOH: &\quad K_a = 1.75 \times 10^{-5} \text{ mole/liter} \\ CH_2FCOOH: &\quad K_a = 1.75 \times 10^{-3} \text{ mole/liter} \\ CHF_2COOH: &\quad K_a = 3.5 \times 10^{-2} \text{ mole/liter} \\ CF_3COOH: &\quad K_a = 1.8 \text{ mole/liter}. \end{aligned} \tag{1.18}$$

Just as inorganic ions affect the dissociation of solvating water, so too can ionized groups in a large molecule affect dissociation of other ionizable groups in the same molecule. The dicarboxylic acid sequence (oxalic, malonic, succinic, glutaric, ...),

$$HOOC - (CH_2)_n - COOH \qquad (n = 0, 1, 2, 3, \ldots) \tag{1.19}$$

exhibits distinct acidity constants for its first and second proton losses. As n increases, the unfavorable electrostatic interaction between charged ends decreases, so in fact the two ionization constants approach one another.

Conjugate to acid dissociation in water would be association of protons with bases such as primary amines:

$$R - NH_2 + H^+ \rightleftharpoons R - NH_3^+. \tag{1.20}$$

Amino acids offer the possibility of both types of reaction occurring in the same molecule, with formation of "zwitterions" with large dipole moments; in the case of the simplest amino acid, glycine, one finds that the intramolecular proton transfer

$$NH_2 - CH_2 - COOH \rightleftharpoons {}^+NH_3 - CH_2 - COO^- \tag{1.21}$$

is virtually complete at the isoelectric point (pH = 6.064).

A degenerate form of internal proton transfer exists in *o*-aminobenzoic acid, in which the proton of the acid group can geometrically hydrogen-bond to the neighboring nitrogen atom without the necessity for dissociation:

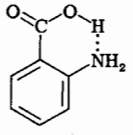

(1.22)

This possibility does not exist for the meta and para forms. Thus the ortho acid is stabilized in its undissociated form, and has the smallest K_a. At 25°C,

$$\begin{aligned} \text{ortho:} \quad & K_a = 1.07 \times 10^{-7} \text{ mole/liter} \\ \text{meta:} \quad & K_a = 1.67 \times 10^{-5} \text{ mole/liter} \\ \text{para:} \quad & K_a = 1.2 \times 10^{-5} \text{ mole/liter.} \end{aligned} \tag{1.23}$$

Dissociation of organic acids can be accompanied by substantial shifts in their electronic excitation spectra. This fact, of course, permits optical spectroscopy to be used to monitor the dissociation degree under various solution conditions. It also leads to the possibility of using strongly absorbing and fluorescing dyes in low concentration as colorimetric pH indicators. Standard indicators are available for use in the pH range 0–14 (Weast, 1975).

Nuclear magnetic resonance (NMR), especially for protons, has also been widely applied to determine acid dissociation in water. The technique has been particularly useful for the study of strong acids such as HCl. In view of the rapidity of proton exchange for such acid solutions, these nuclei give a single resonance signal which is characteristic of the time-averaged environment in which they reside. In these studies, it has been traditional to suppose that dissociation invariably leads to formation of the hydronium ion H_3O^+ (Pople *et al.*, 1959):

$$HA + H_2O \rightleftharpoons H_3O^+ + A^-. \tag{1.24}$$

We shall examine the validity of this solvation assumption later (Sections II and III).

It should also be noted that Raman scattering measurements can be used to observe dissociation of strong acids in concentrated solutions (Young *et al.*, 1959). Discrepancies between NMR and Raman results are occasionally observed and may reflect inadequacy of the proton-solvation hypothesis underlying Eq. (1.24).

In those cases for which proton resonance frequencies in NMR experiments are comparable to their exchange frequencies, lineshapes and positions can be used to determine those exchange rates. Grunwald *et al.* (1957) have exploited this possibility to study the protolysis kinetics of aqueous methylammonium chloride solutions. In the pH range 3–5, they inferred that the proton exchange process

$$CH_3NH_3^+ + CH_3NH_2 \rightleftharpoons CH_3NH_2 + CH_3NH_3^+ \tag{1.25}$$

proceeded through two parallel paths, with roughly equal probability. One path was the direct proton transfer between amines; the other utilized an intervening water molecule or chain of water molecules. Transport of the excess proton thus seems frequently to employ the same basic mechanism that is important in electrochemical transport of protons.

Many chemical reactions in water are specifically catalyzed by hydrogen ions. The hydrolysis of β-propriolactone offers a good example (Long and Purchase, 1950):

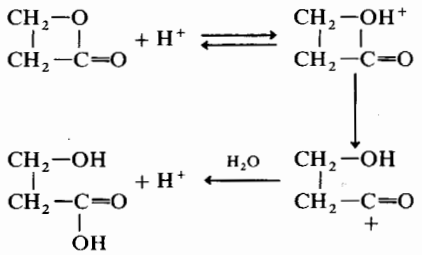

(1.26)

In this case, ring opening precedes addition of the water molecule, perhaps because of ring strain. But with γ-butyrolactone the corresponding proton-catalyzed hydrolysis appears to involve water complexation before ring opening (Long *et al.*, 1951).

Rates of hydrolysis reactions that are specifically catalyzed by hydrogen ions may themselves be used to measure the strengths of acids. Having established the relevant rate constants by prior studies, the degree of dissociation of a given acid in water can be determined by its catalytic power; the stronger the acid, the greater its catalytic action.

Biochemistry provides a large number of important proton transfer reactions. The enzyme carbonic anhydrase, which catalyzes hydration of CO_2 and dehydration of HCO_3^- (or H_2CO_3) offers a prominent example. It contains a zinc atom at its active site, to which a water molecule is strongly bound. It has been proposed that this water molecule and others neighboring it from a chain of hydrogen bonds along which rapid proton transfer occurs in the course of the catalyzed reactions. Finney (1977) has reviewed this and related proposals for the action of other hydrolytic enzymes.

The photochemical action of bacteriorhodopsin involves proton transfer (Stoeckenius, 1976). This purple pigment, found in *Halobacterium halobium*, is a membrane-bound protein. Under illumination, it pumps protons across the membrane to create a potential gradient. The resultant stored energy eventually is used to synthesize the energy-rich molecule ATP that is central to the organism's metabolism.

Finally it should be mentioned that tautomeric proton transfer in nucleotide bases, leading to anomalous base pairing in DNA, has been proposed as a mechanism for spontaneous and induced mutation (Dogonadze *et al.*, 1976).

II. Potential Energy Surfaces

A. Bond Breakage

We now examine in detail the elementary process of dissociation for a single water molecule. Specifically, we inquire into the change in electronic ground state energy of the isolated water molecule as the length r of one of its OH bonds adiabatically elongates to infinity. This process is illustrated in Fig. 3. The bond stretch will be carried out with the other OH bond length and the bond angle held fixed at their equilibrium values (0.9584 Å, 104.45°).

The fragments produced in vacuum by the bond stretch are the H atom and OH radical, rather than H^+ and OH^- ions. The OH radical has equilibrium bond length equal to 0.9699 Å (Herzberg, 1950), so in fact the one produced by the process shown in Fig. 3 is slightly compressed.

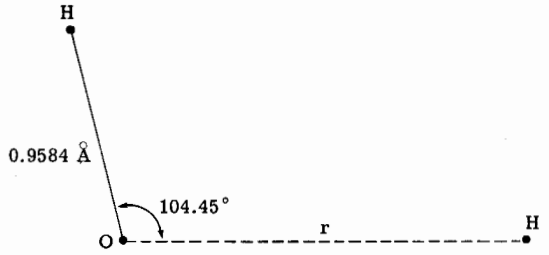

Fig. 3. Water molecule dissociation by single bond stretch. The HOH bond angle and the undeformed bond length retain their equilibrium values, 104.45° and 0.9584 Å, respectively.

Let $E_0(r)$ be the bond stretch energy, which vanishes at $r_e = 0.9584$ Å. For r near r_e an expansion in powers of $r - r_e$ is appropriate:

$$E_0(r) = K_2(r - r_e)^2 + K_3(r - r_e)^3 + K_4(r - r_e)^4 + \cdots. \tag{2.1}$$

There is no reason to doubt that this series has a nonzero radius of convergence. Spectroscopic values are known for the first three coefficients (Smith and Overend, 1972):

$$\begin{aligned} K_2 &= 4.218 \times 10^5 \text{ dyn/cm} \\ K_3 &= -9.57 \times 10^{13} \text{ dyn/cm}^2 \\ K_4 &= 15 \times 10^{21} \text{ dyn/cm}^3. \end{aligned} \tag{2.2}$$

Extraction of higher order terms from either experiment or theory becomes increasingly difficult as the order increases.

As r decreases toward zero, the movable hydrogen nucleus begins to form a "united atom" with the oxygen nucleus. In this limit

$$E_0(r) = (8e^2/r) - C_0 + O(r), \tag{2.3}$$

where the constant C_0 is related to the ground state energy of a hydrogen fluoride molecule with bond length r_e.

The recommended experimental value for the bond dissociation energy in the gas phase process (at 0°K)

$$H_2O \longrightarrow OH + H \tag{2.4}$$

is 118.0 kcal/mole (Darwent, 1970). This energy includes zero-point vibrational contributions from both H_2O and OH. These latter energies are known to be 13.25 kcal/mole for H_2O (Eisenberg and Kauzmann, 1969) and

5.29 kcal/mole for OH (Chamberlain and Roesler, 1955). Combining these values we conclude that

$$\begin{aligned} E_0(\infty) &= 125.96 \text{ kcal/mole} \\ &= 8.7474 \times 10^{-12} \text{ erg/molecule} \\ &= 5.4601 \text{ eV}. \end{aligned} \tag{2.5}$$

Since uncharged fragments are involved, one should expect this limiting value to be approached rapidly with increasing r, probably with exponential order. *Ab initio* quantum-mechanical calculations have not been very successful in attempts to reproduce result (2.5) (Peterson and Pfeiffer, 1972).

The ground electronic state of the water molecule is not the only state that gives unexcited H and OH fragments in the infinite-r limit. Two other excited states of H_2O, a singlet and triplet, will adiabatically produce the same fragments. The corresponding curves of course all lie above $E_0(r)$ for all finite values of r.

The ionization potential of the H atom is 13.530 eV, while the electron affinity of OH is 1.83 $\pm$ 0.04 eV (Berry, 1969). Consequently 11.70 $\pm$ 0.04 eV (269.9 $\pm$ 0.9 kcal/mole) is required to transform the isolated particles H and OH, to H^+ and OH^- by electron transfer. These ionic fragments represent the infinite-r fragments for yet another set of electronic energy curves. From Eq. (2.5) we see that about

$$\begin{aligned} 5.46 + 11.70 &= 17.16 \text{ eV} \\ &= 395.9 \text{ kcal/mole} \end{aligned} \tag{2.6}$$

is the amount of energy that must be expended to produce ionic dissociation of a single water molecule in vacuum. The calorimetric heat of (ionic) dissociation displayed earlier in Eq. (1.11) is far smaller, owing to the very large negative energy of solvating H^+ and OH^- ions in water. Indeed it is this solvation energy that causes dissociation in water to proceed exclusively to ionic products rather than H and OH.

Dipole derivative information (obtained from microwave spectra) helps elucidate the charge redistribution in the water molecule at the beginning of the bond stretch shown in Fig. 3. Clough (1976) provides values for derivatives at the equilibrium geometry that can be resolved into contributions parallel ($\|$) and perpendicular ($\perp$) to the dipole axis of the undeformed molecule:

$$\begin{aligned} (\partial\mu/\partial r)_{\|} &= 0.1568 \times 10^{-10} \text{ esu}, \\ (\partial\mu/\partial r)_{\perp} &= 0.7021 \times 10^{-10} \text{ esu}. \end{aligned} \tag{2.7}$$

One should expect substantially larger values for these effective charges when other water molecules are present to solvate the fragments.

We turn next to an examination of the specific solvation structures produced in water around the ionic H^+ and OH^- dissociation fragments.

B. Hydrated Proton

In order to understand the solvation state of H^+ in liquid water, it is logical first to examine the properties of small hydrate clusters $H^+(H_2O)_n$. These clusters can be generated experimentally in the gas phase, and their thermodynamic properties can be measured (Kebarle *et al.*, 1967). Furthermore, for small n at least, it is possible to carry out reasonably accurate quantum-mechanical calculations to determine structures (Newton and Ehrenson, 1971).

The singly hydrated proton ($n = 1$) is isoelectronic with the ammonia molecule. Therefore it is not surprising that the resulting hydronium ion H_3O^+ is pyramidal, and has C_{3v} symmetry, just as NH_3 does. Kollman and Bender (1973) have carried out *ab initio* quantum-mechanical calculations on the ground electronic state of H_3O^+, with an accuracy claimed to be near the Hartree–Fock limit. The stable C_{3v} structure obtained in their investigation has OH bond lengths equal to 0.963 Å, and HOH angles equal to 112.5°. In comparison with the water molecule geometry, these parameters suggest an enhanced effect of proton–proton repulsion, as might well have been expected in a cationic complex.

Kollman and Bender's study indicates that the inversion barrier (for the $C_{3v} \rightarrow D_{3h} \rightarrow C_{3v}$ transformation) in H_3O^+ lies in the range 2–3 kcal/mole. This is substantially lower than the corresponding barrier height 5.78 kcal/mole in the ammonia molecule (Swalen and Ibers, 1962). Kollman and Bender present energy results calculated for several configurations near the indicated stable point, from which an approximate potential surface could partially be reconstructed.

After accounting for the energy of zero-point nuclear motion, Kollman and Bender estimate from their calculations that the proton affinity of H_2O is 167.5 kcal/mole, and that the deuteron affinity of D_2O (to form D_3O^+) is 170 kcal/mole. The former agrees moderately well with van Raalte and Harrison's value (151 ± 3 kcal/mole) obtained experimentally by gas phase mass spectrometry (van Raalte and Harrison, 1963). The D_2O value is significantly smaller than the estimate 184 ± 7 kcal/mole proposed by DePas *et al.* (1968) also on the basis of mass spectrometry.

The H_3O^+ grouping has been identified in several hydrate crystals. Needless to say, one expects its structure to be subject to significant geometric distortions due to crystal forces. Nevertheless the available crystal data seem to indicate a preference to adhere to the cited pyramidal C_{3v} shape,

thereby confirming the conclusions based on quantum-mechanical calculations. Some of the relevant crystal information has been critically discussed by Almlöf and Wahlgren (1973).

The doubly hydrated proton, $H_5O_2^+$, has been examined theoretically by Newton and Ehrenson (1971) and by Kraemer and Diercksen (1970). Both groups utilized approximate Hartree–Fock solutions to the electronic wave equation. These independent studies agree that $H_5O_2^+$ consists of two water molecules (with antiparallel dipole directions and perpendicular molecular planes) connected by a short symmetrical hydrogen bond. The structure has symmetry D_{2d} and is illustrated in Fig. 4. Owing to a difference in the

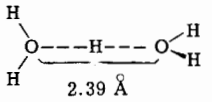

Fig. 4. Stable structure inferred for $H_5O_2^+$ from *ab initio* quantum-mechanical calculations. The terminal water molecules reside in mutually perpendicular planes, both of which contain the central bridging hydrogen.

respective sets of basis functions, the short O–O bond lengths are slightly different in the two studies; Newton and Ehrenson find 2.36 Å, while Kraemer and Diercksen obtain 2.39 Å. There seems to be little doubt that the bridging hydrogen is the one still to be regarded as "the hydrogen ion," since unlike the four other hydrogens it is significantly farther from either oxygen than the normal OH covalent bond length in the water molecule.

The short symmetrical hydrogen bond in $H_5O_2^+$ is closely analogous to the one that exists in the isoelectronic bifluoride anion, FHF^-. At least in the former, Kraemer and Diercksen point out that the bridging proton moves in a very flat potential well along the O–O axis, which no doubt must be relevant to ease of H^+ transport in an extended aqueous medium.

In addition to displacement of the bridging hydrogen, certain other distortions of the $H_5O_2^+$ structure shown in Fig. 4 can occur at relatively low energy cost. In particular, it is easy to rotate one of the terminal H_2O units about its oxygen so as to produce a pyramidal arrangement with the central hydrogen. Thus one readily converts the symmetrical structure shown to an asymmetrical $(H_3O^+)H_2O$, a singly hydrated pyramidal hydronium ion.

The energy of addition of a second water molecule to H_3O^+ to form $H_5O_2^+$ is far less than the energy of the first hydration of H^+ quoted above. Kraemer and Diercksen find this second binding energy to be 32.24 kcal/mole, compared to the experimental value 35.4 kcal/mole (Kebarle *et al.*, 1967).

The crystal structures of several acid hydrates reveal the presence of $H_5O_2^+$. Perchloric acid dihydrate offers a good example (Olovsson, 1968). In this crystal the bridged oxygen–oxygen distance is observed to be 2.424 Å.

Interactions of the $H_5O_2^+$ ions within the solid distort them from the D_{2d} symmetry presumed to obtain for the isolated species. $H_5O_2^+$ ions with different distortions (but similar short O–O distances) occur in the di- and trihydrate crystals of HCl (Lundgren and Olovsson, 1967).

The most systematic quantum-mechanical study of higher hydrates of H^+ has been carried out by Newton and Ehrenson (1971). They were able to perform geometry searches, in varying degrees of completeness, for ions up to $H^+(H_2O)_5$. The complexes studied tended always to exhibit shorter hydrogen bonds than would exist in the corresponding uncharged clusters of water molecules without the extra proton.

In the case of $H^+(H_2O)_3$ (i.e., $H_7O_3^+$) Newton and Ehrenson concluded that the most stable structure is "open," not "cyclic." It can best be described as a flattened H_3O^+, two protons of which form hydrogen bonds to pendant H_2O's. The resulting complex has C_{2v} symmetry, and its two equivalent O–O distances are found to be 2.46 Å. Although subject to the distortive effect of crystal forces, these open $H_7O_3^+$ cations have also been observed in solid hydrates (Almlöf, 1972).

The symmetrically hydrated hydronium ion $H_3O^+(H_2O)_3$ (or $H_9O_4^+$) has been prominently advocated as an important chemical species in liquid water (Eigen and DeMaeyer, 1958). The original suggestions indicated that this species ought to be pyramidal, following the presumed shape of H_3O^+. However, Newton and Ehrenson find that the stable isolated $H_9O_4^+$ has incorporated a flattened H_3O^+ unit to yield symmetry D_{3h}. Figure 5 shows

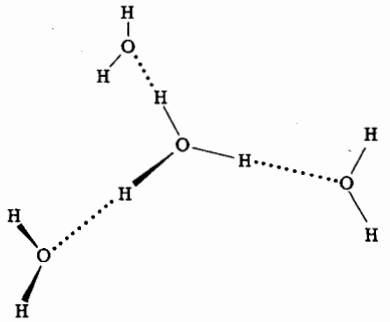

Fig. 5. Lowest energy configuration for $H_9O_4^+$ (Newton and Ehrenson, 1971). The three terminal water molecules are each perpendicular to the plane of the flattened central H_3O^+.

its structure. The three equivalent O–O distances are found to be 2.54 Å. No doubt the flattening present in $H_9O_4^+$ must be due to repulsions between the pendant H_2O's; nevertheless, the energy required to reintroduce pyramidal distortion of significant magnitude is probably small.

The grouping $H_9O_4^+$ is found in crystals of hydrogen bromide tetrahy-

drate (Lundgren and Olovsson, 1968), along with $H_7O_3^+$. The former complex has O–O distances 2.496 Å, 2.587 Å, and 2.588 Å, and exhibits pyramidal distortion.

Insufficient quantum-mechanical information is available at present to draw any firm conclusions about the minimum-energy structure of $H^+(H_2O)_5$ (i.e., $H_{11}O_5^+$). This cationic unit has not been identified yet in hydrate crystals, although it has been observed in irradiated water vapor (Kebarle *et al.*, 1967).

The largest proton hydrate unit that has thus far been identified in the solid state is $H_{13}O_6^+$. This cation is formed when the cage compound $[(C_9H_{18})_3(NH)_2Cl]^+Cl^-$ is crystallized from hydrochloric acid solution (Bell *et al.*, 1975). The $H_{13}O_9^+$ structure displays a very short central hydrogen bond (2.39 Å between oxygens) along which a bridging proton is presumed to be symmetrically placed. The outer O–O hydrogen bonds are 2.52 Å long. The best description of the cation is that it consists of an $H_5O_2^+$ unit, with each of the four pendant hydrogens bonded to single water molecules. No doubt the $H_{13}O_6^+$ observed in the crystal is considerably distorted from its optimal gas-phase geometry.

Probably the two major conclusions to be drawn from the information cited are (a) the extra proton in water clusters tends to produce substantially shortened hydrogen bonds, and (b) the cationic complexes are easily distorted from their most stable configurations. Extrapolating to the limit of infinite solvation degree ($n \to \infty$), we can expect these two conclusions to apply to excess protons in bulk liquid water. In order for the position of the excess proton to change substantially, the region of shortened hydrogen bonding must likewise shift; these concerted positional shifts are aided by ease of structural distortion induced by presence of the excess proton.

C. Hydrated Hydroxide

We turn now to consideration of the anionic complexes $OH^-(H_2O)_n$. Unfortunately, these seem to be rather difficult to generate in the gas phase, so virtually no experimental information is presently available for these species.

As a point of reference, note that the equilibrium bond length for the isolated OH^- is close to the bond length in H_2O. Janoschek *et al.* (1967) report 0.963 Å for an accurate Hartree–Fock calculation for OH^-.

Once again, the most systematic quantum-mechanical study of the hydrated ions is due to Newton and Ehrenson (1971). Their optimized structure for the monohydrate species $H_3O_2^-$ is illustrated in Fig. 6. This anion is found to be planar, with a relatively short O–O distance, 2.45 Å. However the hydrogen bond is asymmetric, with two equivalent positions for the central proton, separated by 0.23 Å. The double-well potential in which the

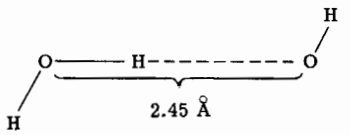

Fig. 6. Optimal structure for $H_3O_2^-$, according to Newton and Ehrenson (1971). The bonding central proton resides at one of the minima in a double-well potential.

proton moves has a predicted barrier height of about 0.13 kcal/mole. The energy of single hydration of OH^- is calculated to be 40.73 kcal/mole.

It is instructive to compare the $H_3O_2^-$ structure with the analogous cation $H_5O_2^+$. Although both incorporate short hydrogen bonds, the anion has apparently a significantly longer one (by 0.09 Å in the Newton–Ehrenson study). This lengthening may explain the existence of a double-minimum potential for the bridging proton in the anion, compared to the very flat potential in the cation. This distinction also may be relevant to the mobility difference between H^+ and OH^- in liquid water that appears in Table II, since it suggests that proton transfers near an excess proton are less frequently retarded by potential barriers than proton transfers near a missing proton ("protonic hole").

The optimized structure found for $H_5O_3^-$ by Newton and Ehrenson is planar, with symmetry C_{2v}. The OH^- acts as proton acceptor for both hydrating water molecules, with equivalent O–O bond lengths of 2.53 Å. Once again this anion length is significantly greater than that found in the same study for the corresponding cation $H_7O_3^+$, namely 2.46 Å.

The trihydrate species $H_7O_4^-$ in the Newton–Ehrenson study achieves greatest stability in a branched structure with each of the water molecules contributing a proton in a hydrogen bond to the central OH^-. The specific configuration of this type studied had C_{3v} symmetry, with the three hydrogen bonds forming a pyramidal shape (with vertex angles for oxygen equal to 110°). The O–O distances were optimized at 2.61 Å, again larger than the 2.54 Å found for the corresponding $H_9O_4^+$ (Fig. 5). It would eventually be desirable to study the change in energy of this branched structure with respect to flattening of the pyramid to see how readily external perturbations could induce such shape changes.

Newton and Ehrenson also carried out preliminary study of the tetrahydrate $H_9O_5^-$ but without sufficient detail and flexibility in configurational options to permit firm conclusions to be drawn.

Overall, the hydrated OH^- complexes seem to involve longer hydrogen bonds and more inflexibility toward rearrangement than the analogous hydrated H^+ complexes. The tendency toward greater bond lengths seems to be supported by crystallographic data, when the previously cited acid

hydrates are compared with substances such as sodium hydroxide hydrates (Beurskens and Jeffrey, 1964) and tetramethylammonium hydroxide pentahydrate (McMullan *et al.* 1966).

III. General Theory of Association–Dissociation Reactions

A. Definition of Chemical Species

Results presented in the preceding section suggest that solvated H^+ and OH^- may exist in water with considerable diversity in local structure. Therefore, it may be quite misleading to describe the solution behavior of these ions in terms of discrete chemical entities, such as the frequently mentioned hydronium ion H_3O^+. To avoid unnecessary committment to specific chemical structures, we will now develop a general procedure for description of the dissociation and solvation processes in water. Some elements of this formalism have been advanced previously (Stillinger, 1975).

The central problem is this: Given a set of nuclear positions, $\mathbf{r}_1 \cdots \mathbf{r}_N$ for oxygens, $\mathbf{r}_{N+1} \cdots \mathbf{r}_{3N}$ for hydrogens, attribute all of these nuclei uniquely to H_2O, OH^-, and H^+ species. [We disregard the possible existence of O^{2-}, produced by double dissociation, on physical grounds.] The attribution will be based on the set of oxygen–hydrogen distances produced by $\mathbf{r}_1 \cdots \mathbf{r}_{3N}$.

The only element of arbitrariness to be introduced concerns the choice of a bond dissociation distance L, such that any oxygen–hydrogen pair whose distance exceeds L is never regarded as bonded, either in an H_2O or an OH^- species. A reasonable choice for L seems to be

$$L = 1.375 \text{ Å}. \tag{3.1}$$

This is half the distance between neighboring oxygen nuclei in ice at 0°K and zero pressure and would surely be the natural distance choice for proton assignment to oxygens in that crystal. Note that use of the first three terms in formula (2.1) presented earlier for bond stretching indicates that about 70 kcal/mole are required to increase the normal OH bond in water to length L. Of course this is relevant only for the absence of all other water molecules; their presence would normally reduce the energy needed for bond stretch.

The number of OH pairs of any distance is exactly $2N^2$. We will denote these distances by $l(i, j)$, where i and j are running indices referring, respectively, to oxygens and hydrogens,

$$\begin{aligned} 1 \leq i \leq N, \\ N + 1 \leq j \leq 3N. \end{aligned} \tag{3.2}$$

Except in the event of zero-probability coincidences, the distances may be ordered in an ascending sequence:

$$l(i_1, j_1) < l(i_2, j_2) < \cdots < l(i_M, j_M), \qquad M = 2N^2. \tag{3.3}$$

Of course each i appears $2N$ times in this sequence, and each j appears N times. The order of appearance depends on the set of positions $\mathbf{r}_1 \cdots \mathbf{r}_{3N}$. In a macroscopic system with a relatively uniform matter distribution, the majority of distances appearing in the sequence (3.3) will have macroscopic magnitudes.

We will be concerned only with the subset of distances obeying the inequality

$$l(i_\alpha, j_\alpha) < L. \tag{3.4}$$

These distances *might* correspond to chemical bonds within the species H_2O and OH^-, but they need not. We shall employ the following "bonding" algorithm for the ordered distance subset obeying (3.4).

1. Bond the two nuclei that provide the minimum distance in the subset list.
2. Remove from the list all distances that involve hydrogens previously bonded and/or involve oxygens bonded twice previously.
3. Return to step 1 if any distances remain in the list.

After this algorithm has exhausted the distance list, the resulting "bonds" will have formed H_2O molecules (2 OH bonds), OH^- ions (1 OH bond), and a certain number of H^+ ions will be left over. Notice that the algorithm does not permit any oxygen to bond to more than two hydrogens, nor does it permit any hydrogen to bond simultaneously to more than a single oxygen. Unbonded H^+ ions may actually be closer to oxygens than the broken bond distance L, but for them to have remained unbonded it is necessary that those oxygens be bonded to pairs of even closer hydrogens.

As time proceeds, the nuclear positions $\mathbf{r}_1 \cdots \mathbf{r}_{3N}$ naturally will change. This will affect OH distances, and consequently the result of the bonding convention will differ. In particular, the number N_w of intact water molecules, of hydroxide anions N_-, and of hydrogen ions N_+ will fluctuate with time t. Of course at all times we have

$$\begin{aligned} N_w(t) &= N - N_+(t), \\ N_-(t) &= N_+(t). \end{aligned} \tag{3.5}$$

There is a variety of ways that bond exchanges can occur (i.e., exchanges of hydrogens between oxygens) without any net change in N_w, N_+, or N_-.

The simplest possibility consists of close approach of H^+ to a water molecule. If this H^+ moves closer to the oxygen atom of the molecule than the larger of its two initial OH bond lengths, then the bonding algorithm requires the new OH distance to be identified as one of the intramolecular bonds. At the same time, the furthest hydrogen of the three loses its bond to the oxygen, and by definition now becomes the unbonded H^+. This transformation is illustrated in Fig. 7.

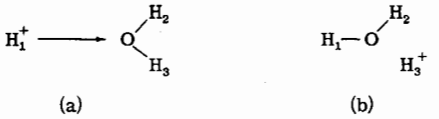

Fig. 7. Bond exchange process for proton approach to a water molecule. (a) The proton at the left is farther from the oxygen than either intramolecular OH bond length. (b) Motion has reduced the initially large distance to a value smaller than one of the original OH bond lengths, thereby requiring re-identification of bonded pairs.

A somewhat more complex bond exchange, involving two water molecules, is shown in Fig. 8. The two molecules possess four internal (intramolecular) bonds; there are in addition four intermolecular OH distances. For any set of bonds assigned by our algorithm, the largest of the first four must be smaller than the smallest of the latter four. If this were not so, the bonding algorithm would have identified the bonds differently. As shown in Fig. 8, a close collision between the two water molecules can require change in bonding, so as to restore compliance with the stated inequality between four intramolecular and four intermolecular distances. As in the preceding simpler case, the new bonding scheme may or may not persist for a substantial length of time, depending on the subsequent motions of the nuclei.

It must also be stressed that under the bonding algorithm, processes exist which involve cooperative bond shifts along a sequence of molecules, which are not themselves required to move to cause these shifts. Figure 9 shows how this can occur; H^+ "attacks" one end of a water molecule chain (along which OH distances increase), and by forcing redrawing of OH bonds, it

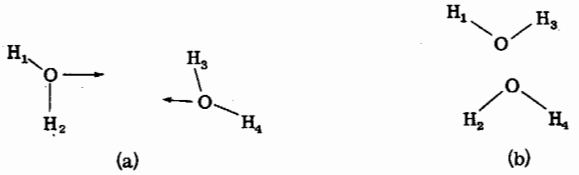

Fig. 8. Simultaneous exchange of hydrogens between two water molecules in a close collision.

succeeds in "freeing" H^+ at the other end. Needless to say, a version of the shift presented in Fig. 9 exists for an excess hydroxide ion, rather than the case shown of an excess proton. One recognizes that the more molecules participating, the rarer will be the configurational circumstances required.

Especially when examining a cooperative shift such as that indicated in Fig. 9, it is important to realize that charge is not discontinuously transported at the instant of rebonding. Of course, electrostatic charge density in

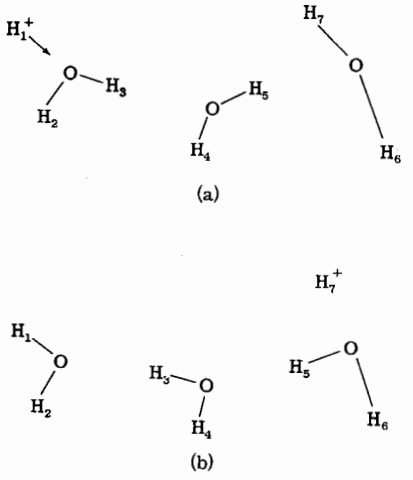

Fig. 9. Cooperative bond transfer along a sequence of molecules, resulting in a different location for the excess proton.

the system is a continuous function of nuclear positions. Under most circumstances we expect excess charge to be localized at or near the ion identified by the bonding algorithm; however, the special molecular arrangements and distortions required by Fig. 9 may tend to delocalize charge over several molecules.

The sequential charge transport illustrated earlier in Fig. 1 stands in distinction to the rate process of Fig. 9. The former requires all intervening protons to move, which in turn causes occurrence of a sequence of simple formal bond shifts.

In addition to the formal exchange processes which conserve N_w, N_+, and N_-, there is a variety of association and dissociation processes encompassed within our bonding scheme which change these species numbers. Just as before, these can be simple, or they can require the cooperative involvement of several intervening molecules. We shall consider these association and dissociation reactions at some length in Section III,C below.

B. Molecular Distribution Functions

Having now introduced an unambiguous identification procedure for intact water molecules and ionic H^+ and OH^- fragments, we next outline a molecular distribution function formalism to describe these species in the liquid phase. The desirability for having such a formalism stems primarily from the inevitable variability in solvation structures around the ions, and from the importance of that variability in affecting kinetics of transport and reaction of those ions. For simplicity of presentation we shall initially use *classical* statistical mechanics. With particles as light as protons it is of course necessary really to use *quantum* statistical mechanics, so at the end of this development the procedure for effecting the necessary modifications will be indicated.

In order to describe the instantaneous configuration of a given water molecule α, we shall use a nine-vector $\mathbf{x}_\alpha$. This comprises full specification of the three nuclear positions. For each of the unbonded protons, only three-vectors are necessary, to be denoted by $\mathbf{s}_\beta$. Six-vectors $\mathbf{t}_\gamma$ will be employed for the hydroxide ions.

The statistical-mechanical theory can be most conveniently developed for the grand ensemble (Hill, 1956). The appropriate generating function is the grand parition function Z_G. We shall initially treat the concentrations of each of H_2O, H^+, and OH^- as independent and therefore we introduce the respective absolute activities y_w, y_+, and y_- as independent parameters. This strategem implies an ability to block attainment of the usual association–dissociation equilibrium between the three species. However, that does not mean we forego knowledge about that equilibrium, because at some later stage we can simply look for a maximum in the grand potential subject to the constraint

$$N_+ = N_-, \tag{3.6}$$

and then identify the concentrations as those appropriate to equilibrium.

The grand partition function has the following form:

$$Z_G = \sum_{N_w, N_+, N_- = 0}^{\infty} \frac{y_w^{N_w} y_+^{N_+} y_-^{N_-}}{(2!)^{N_w} N_w! N_+! N_-!} \times \int d\mathbf{x}_1 \cdots \int d\mathbf{t}_{N_-} \exp[-\beta\Phi(\mathbf{x}_1 \cdots \mathbf{x}_{N_w} | \mathbf{s}_1 \cdots \mathbf{s}_{N_+} | \mathbf{t}_1 \cdots \mathbf{t}_{N_-})],$$

$$\beta = (k_B T)^{-1}. \tag{3.7}$$

Here Φ represents the potential energy (i.e., the ground-electronic state energy hypersurface) for the nuclear configuration specified by $\mathbf{x}_1 \cdots \mathbf{t}_{N_-}$. The denominator factor $(2!)^{N_w}$ in Eq. (3.7) must be inserted to account for proton indistinguishability in each water molecule. Integrations must be

restricted to that portion of configuration space which corresponds to bonding of nuclei into the given numbers of molecules and ions, according to the foregoing bonding algorithm.

The connection between Z_G and thermodynamic properties (at least when the system is essentially electrically neutral), is provided by the identification

$$\ln Z_G = \beta p V, \tag{3.8}$$

where p is the pressure and V is the volume. From Eq. (3.7) it is easy to see that the average numbers of each of the three species present can be obtained from activity derivatives of $\ln Z_G$:

$$\begin{aligned}
\langle N_w \rangle &= \left(\frac{\partial \ln Z_G}{\partial \ln y_w} \right)_{\beta, y_+, y_-}, \\
\langle N_+ \rangle &= \left(\frac{\partial \ln Z_G}{\partial \ln y_+} \right)_{\beta, y_w, y_-}, \\
\langle N_- \rangle &= \left(\frac{\partial \ln Z_G}{\partial \ln y_-} \right)_{\beta, y_w, y_+}.
\end{aligned} \tag{3.9}$$

In particular, the functional relation between hydrogen ion concentration and the activity y_+ provided by these identities constitutes a formal way to determine pH in the liquid.

Next we introduce molecular distribution functions $\rho^{(n_w, n_+, n_-)}$, to describe the occurrence probabilities in the system of sets comprising n_w water molecules, n_+ hydrogen cations, and n_- hydroxide anions, in specified configurations. The formal definition of these quantities in the grand ensemble is as follows:

$$\begin{aligned}
&\rho^{(n_w, n_+, n_-)}(\mathbf{x}_1 \cdots \mathbf{x}_{n_w} | \mathbf{s}_1 \cdots \mathbf{s}_{n_+} | \mathbf{t}_1 \cdots \mathbf{t}_{n_-}) \\
&\quad = Z_G^{-1} \sum_{N_w, N_+, N_-} \frac{y_w^{N_w} y_+^{N_+} y_-^{N_-}}{(2!)^{N_w} (N_w - n_w)! (N_+ - n_+)! (N_- - n_-)!} \\
&\qquad \times \int \cdots \int d\mathbf{x}_{n_w+1} \cdots d\mathbf{x}_{N_w} \, d\mathbf{s}_{n_+ + 1} \cdots d\mathbf{s}_{N_+} \, d\mathbf{t}_{n_- + 1} \cdots d\mathbf{t}_{N_-} \\
&\qquad \times \exp[-\beta \Phi(\mathbf{x}_1 \cdots \mathbf{t}_{N_-})].
\end{aligned} \tag{3.10}$$

The singlet distribution function $\rho^{(0,1,0)}(\mathbf{s})$ is equal to the hydrogen ion concentration at position $\mathbf{s}$. In the case of the corresponding hydroxide function $\rho^{(0,0,1)}(\mathbf{t})$, $\mathbf{t}$ specifies not only position, but orientation and bond length as well, so that this function specifies local density of anions of given orientation and degree of bond stretch. Only after integration over these two internal degrees of freedom will $\rho^{(0,0,1)}(\mathbf{t})$ yield the local concentration of OH^-. Similarly the singlet water molecule distribution function $\rho^{(1,0,0)}(\mathbf{x})$

specifies local density of molecules with given position, orientation, and deformation. In liquid water, rotational and translational symmetry applies to the three singlet distribution functions, except possibly near perturbing boundaries.

In the general case of arbitrary (nonnegative) n_w, n_+, and n_-, the molecular distribution function $\rho^{(n_w, n_+, n_-)}$ will reduce to a product of singlet functions if all of the $n_w + n_+ + n_-$ particles are widely separated from one another:

$$\rho^{(n_w, n_+, n_-)}(\mathbf{x}_1 \cdots \mathbf{t}_{n_-}) \to \left[\prod_{i=1}^{n_w} \rho^{(1,0,0)}(\mathbf{x}_i)\right] \times \left[\prod_{j=1}^{n_+} \rho^{(0,1,0)}(\mathbf{s}_j)\right] \times \left[\prod_{k=1}^{n_-} \rho^{(0,0,1)}(\mathbf{t}_k)\right]. \tag{3.11}$$

This asymptotic factorization remains true even if the water is crystalline, for which spatially periodic singlet functions obtain.

The pair molecular distribution functions convey fundamental information about structure in the liquid, and about the nature of H^+ and OH^- solvation. For subsequent purposes it will be most convenient to consider these distribution functions only in the infinite-system-size limit, so that boundary effects do not appear. There exists an obvious set of exact relations, the "local electroneutrality conditions," which must be satisfied by the pair distribution functions. These conditions state that because a partially dissociated liquid is electrically conducting, any charge within the liquid is exactly neutralized (shielded) by an average diffuse accumulation of local charge of opposite sign. In particular this must be true for an H^+ ion, and the resulting identity is

$$\int d\mathbf{s}_2 \left[\frac{\rho^{(0,2,0)}(s_{12})}{\rho^{(0,1,0)}} - \rho^{(0,1,0)}\right] - \int d\mathbf{t}_1 \left[\frac{\rho^{(0,1,1)}(\mathbf{s}_1, \mathbf{t}_1)}{\rho^{(0,1,0)}} - \rho^{(0,0,1)}(\mathbf{t}_1)\right] = -1. \tag{3.12}$$

The corresponding statement for the shielding of an hydroxide ion (with fixed configuration $\mathbf{t}_1$) is

$$\int d\mathbf{s}_1 \left[\frac{\rho^{(0,1,1)}(\mathbf{s}_1, \mathbf{t}_1)}{\rho^{(0,0,1)}(\mathbf{t}_1)} - \rho^{(0,1,0)}\right] - \int d\mathbf{t}_2 \left[\frac{\rho^{(0,0,2)}(\mathbf{t}_1, \mathbf{t}_2)}{\rho^{(0,0,1)}(\mathbf{t}_1)} - \rho^{(0,0,1)}(\mathbf{t}_2)\right] = 1. \tag{3.13}$$

Finally, we have a third relation which states that no net ionic charge will accumulate in the vicinity of a water molecule with fixed configuration $\mathbf{x}_1$, since it is uncharged:

$$\int d\mathbf{s}_1 \left[\frac{\rho^{(1,1,0)}(\mathbf{x}_1, \mathbf{s}_1)}{\rho^{(1,0,0)}(\mathbf{x}_1)} - \rho^{(0,1,0)} \right] - \int d\mathbf{t}_1 \left[\frac{\rho^{(1,0,1)}(\mathbf{x}_1, \mathbf{t}_1)}{\rho^{(1,0,0)}(\mathbf{x}_1)} - \rho^{(0,0,1)}(\mathbf{t}_1) \right] = 0. \quad (3.14)$$

These local electroneutrality conditions can be generalized to provide exact constraints on higher order distribution functions. These generalizations are based on shielding of the total charge of any fixed set of H_2O, H^+, and OH^- particles by the surrounding conductive medium. For present purposes it is unnecessary to dwell upon these generalizations.

In addition to local electroneutrality conditions, the pair distribution functions in a conducting medium are obliged to obey a "second moment condition" (Stillinger and Lovett, 1968). This condition owes its existence to the fact that Coulomb interactions drop off only as inverse distance with increasing separation. We state the second moment condition without proof:

$$\int d\mathbf{r}_{12} r_{12}^2 \left\{ \rho^{(0,2,0)}(r_{12}) - 2 \int d\tau_2 \rho^{(0,1,1)}(\mathbf{r}_1, \mathbf{t}_2) + \int d\tau_1 \, d\tau_2 \rho^{(0,0,2)}(\mathbf{t}_1, \mathbf{t}_2) \right\} = -12C/\kappa^2. \quad (3.15)$$

Here C stands for the common concentration of H^+ and of OH^- ions, and κ is the Debye parameter for the ionic solution:

$$\kappa^2 = 8\pi C e^2/\varepsilon_0 k_B T; \quad (3.16)$$

ε_0 stands for the static dielectric constant of the liquid.

The distance r_{12} appearing in Eq. (3.15) is a distance between two ions. For hydrogen ions there is no ambiguity; this is simply the distance between the hydrogen nuclei. But for hydroxide ions, it is necessary to make a consistent choice of position in that diatomic species for definition of distance. In fact, Eq. (3.15) remains valid whatever convention is chosen (whether it is the O nucleus, or some intermediate point); but in any case the hydroxide six-vector $\mathbf{t}$ must then be resolved into a direct sum of three-vectors:

$$\mathbf{t} = \mathbf{r} \oplus \tau, \quad (3.17)$$

with $\mathbf{r}$ giving the position of the "center" of the hydroxide, and τ specifying

orientation and OH bond length. Note that these latter degrees of freedom are integrated in the second moment condition (3.15).

Owing to the small extent of dissociation in water around room temperature and one atmosphere pressure, the solvated H^+ and OH^- ions constitute a very dilute electrolyte. Consequently, the ionic distribution functions (except at small distances) will accurately be described by the linear Debye–Hückel form (Résibois, 1968):

$$\rho^{(0,2,0)} \sim \rho^{(0,0,2)} \sim C^2[1 - e^2 \exp(-\kappa r_{12})/k_B T\varepsilon_0 r_{12}],$$
$$\rho^{(0,1,1)} \sim C^2[1 + e^2 \exp(-\kappa r_{12})/k_B T\varepsilon_0 r_{12}]. \qquad (3.18)$$

For water at 20°C, the Debye distance $1/\kappa$ is equal to 10,600 Å, which is considerably larger than $C^{-1/3}$, the mean separation between like ions, which equals 2720 Å under the same conditions.

The ion–water and water–water pair distribution functions will approach their long-range limits [described by Eq. (3.11) above] more rapidly than those functions shown in Eq. (3.18); the specific forms involved will exhibit Debye shielding provided the distance is some substantial fraction of $1/\kappa$.

Details about H^+ and OH^- solvation are primarily contained in the pair functions $\rho^{(1,1,0)}$ and $\rho^{(1,0,1)}$. The form of the first of these bears directly on validity of the assumption that solvated protons are predominately present in water as pyramidal hydronium units H_3O^+ (Eigen, 1964). Similarly, the second function would indicate predominance of an analogous pyramidal $OH^-(H_2O)_3$, if such were indeed an apt description of primary hydroxide solvation.

If the primary hydration structure for H^+ in water is principally the pyramidal H_3O^+, then $\rho^{(1,1,0)}$ should be strongly peaked near the configuration shown in Fig. 10a. In particular, this would involve a rather sharp distribution of the $H^+ \cdots O$ distance at about 0.96 Å, and a second

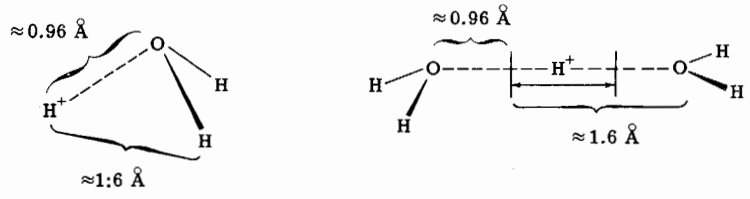

Pyramidal primary hydration (a)

Symmetrically diffuse H^+ bridge (b)

Fig. 10. Primary hydration structures for H^+ in water. The pyramidal "hydronium" in (a) has been advocated by Eigen (1964). Alternative (b) represents a deformable class of proton bridges, with the proton diffusely, but more or less symmetrically, distributed between the participating oxygens.

distinguishable maximum in $H^+ \cdots O$ distances at about 1.6 Å to be consistent with a secondary hydration shell (Eigen, 1964). Furthermore the postulated nonplanarity of the basic H_3O^+ implies that the H^+ is preferentially located about 1.6 Å from the two H's of the water, when this molecule's oxygen is near the cited 0.96 Å distance from H^+.

On the other hand, we have noted in Section II,B that the solvated proton can be (and often is, in crystals) located symmetrically and diffusely along short hydrogen bonds between two essentially equivalent water molecules [Fig. 10b]. If indeed this is the more appropriate description, then $\rho^{(1,1,0)}$ would have to convey a broad single distribution of $H^+ \cdots O$ distances over the range 0.96–1.60 Å, without any marked preference for sharply defined $H^+ \cdots H$ distances.

The water–hydroxide pair distribution function $\rho^{(1,0,1)}$ should possess a strong maximum when the two oxygen atoms are about 2.5 Å apart. Since this represents a strong, short hydrogen bond with the water acting as proton donor, $\rho^{(1,0,1)}$ should achieve its largest value in this distance range in the two equivalent molecular orientations that point covalent OH bonds toward the hydroxide hydrogen. Furthermore, since the hydroxide has no tendency itself to act as proton donor, no significant water molecule probability should be manifest in $\rho^{(1,0,1)}$, along the hydroxide OH bond, at $O \cdots O$ distances in the range 2.5–3.0 Å.

Under those temperature and pressure conditions which lead to small degree of water dissociation, separate partial molar volumes $\overline{V}^0_+$ and $\overline{V}^0_-$ may be attributed to H^+ and to OH^- which reflect the solvation of these individual ions by pure undissociated water. The result (1.12) quoted earlier for the volume of dissociation is essentially composed of the sum of these quantities, both of which are probably negative. Expressions can be written for $\overline{V}^0_+$ and $\overline{V}^0_-$ in terms of singlet and pair distribution functions. For H^+ one derives the following expression:

$$\overline{V}^0_+ = k_B T \kappa_T - \frac{V}{\langle N_w \rangle} \int d\mathbf{x} \left[\frac{\rho^{(1,1,0)}(\mathbf{x}|\mathbf{s})}{\rho^{(0,1,0)}(\mathbf{s})} - \rho^{(1,0,0)}(\mathbf{x}) \right], \qquad (3.19)$$

wherein κ_T stands for isothermal compressibility of water. An exactly analogous expression gives $\overline{V}^0_-$.

The quantum-mechanical extension of the distribution function formalism requires first that one introduce a suitable complete orthonormal set of eigenfunctions. This complete set is necessary to describe motion of all oxygen and hydrogen nuclei on the ground electronic state hypersurface (the Born–Oppenheimer separation of nuclear and electronic motion should be an accurate description). Then the quantum-mechanical grand partition function has the form of an operator trace:

$$\Xi_G = \mathrm{Tr} \exp[-\beta(\mathscr{H} - \mu_O \mathscr{N}_O - \mu_H \mathscr{N}_H)]. \qquad (3.20)$$

Here $\mathscr{H}$ is the nuclear-motion Hamiltonian, $\hat{N}_O$ and $\hat{N}_H$ are number operators for O and H nuclei, respectively, and μ_O and μ_H are the corresponding nuclear chemical potentials.

The bonding algorithm advocated above (Section III,A) partitions multidimensional nuclear configuration space into regions corresponding to the fixed numbers N_w, N_+, N_- of intact molecules, H^+ ions, and OH^- ions. This geometric partitioning effectively defines number operators $\hat{N}_w$, $\hat{N}_+$, and $\hat{N}_-$ for the respective species, so that the averages $\langle N_w \rangle$, $\langle N_+ \rangle$, and $\langle N_- \rangle$ may be obtained quantum-mechanically as suitable traces:

$$\langle N_\alpha \rangle = Z_G^{-1} \operatorname{Tr}\{\hat{N}_\alpha \exp[-\beta(\mathscr{H} - \mu_O \hat{N}_O - \mu_H \hat{N}_H)]\}, \quad \alpha = w, +, -, \tag{3.21}$$

The quantum-mechanical distribution functions corresponding to the classical quantities defined earlier in Eq. (3.10) may also be represented as operator traces. Alternatively, one can consider the full density matrix for the operator

$$\exp[-\beta(\mathscr{H} - \mu_O \hat{N}_O - \mu_H \hat{N}_H)]$$

in coordinate representation, and then produce reduced density matrices by integration. Note, however, that our bonding algorithm requires that the integrations be carried out over rather complicated multidimensional regions.

The passage from classical statistical mechanics to quantum statistical mechanics engenders two basic changes in the molecular description of water. The first concerns zero-point motion, primarily of the light hydrogens, which tends to broaden distribution function maxima (i.e., particles will be somewhat delocalized). Needless to say, this effect will be greatest for the lightest isotopes. The other effect is obvious from Table III, namely, that light-hydrogen-mass quantum effects tend to displace the association–dissociation equilibrium toward ionic products. The implication for singlet distribution functions is obvious, and these in turn affect the higher order distribution functions.

C. Linear Response Theory of Reaction for Pure Water

Our next task is derivation of a fluctuation–dissipation theorem for the dissociation process in liquid water. Although autocorrelation functions for chemical reaction rates have previously been deduced (Kutz *et al.*, 1974), the emphasis and details of the present distinct approach seem to reveal the underlying dynamics more clearly than ever before. We shall develop the purely classical theory first, then we indicate how the quantum-mechanical version can be achieved.

For simplicity, suppose that the system contains precisely N oxygen nuclei and $2N$ hydrogen nuclei. Furthermore let $\mathbf{r}$ and $\mathbf{p}$, respectively, comprise all configuration and momentum coordinates for the $3N$ nuclei. The bonding algorithm presented in Section III, A provides a definition for $N_+(\mathbf{r})$, the number of hydrogen ions to be identified as fragments of dissociated water molecules, for any given $\mathbf{r}$. As stated earlier [Eq. (3.5)], N_+ is the number of hydroxides as well, and $N - N_+$ is the number of undissociated molecules.

Denote by $\Omega(N_+)$ that portion of the full $3N$-dimensional $\mathbf{r}$-space which corresponds to the existence of precisely N_+ hydrogen ions in the liquid. The probability $P(N_+)$ that indeed this is exactly the number of H^+ ions present may be expressed in terms of configuration space integrals in the following obvious way:

$$P(N_+) = \left\{\int_{\Omega(N_+)} d\mathbf{r} \exp[-\beta\Phi(\mathbf{r})]\right\} \Big/ \left\{\sum_{N_+=0}^{N} \int_{\Omega(N_+)} d\mathbf{r} \exp[-\beta\Phi(\mathbf{r})]\right\}. \quad (3.22)$$

Owing to the usual behavior of large numbers, this probability can be adequately represented by a normalized Gaussian distribution:

$$P(N_+) = (K/2\pi)^{1/2} \exp[-\tfrac{1}{2}K(N_+ - \langle N_+\rangle)^2]. \quad (3.23)$$

The quadratic fluctuation is then trivial to calculate:

$$\langle (N_+ - \langle N_+\rangle)^2\rangle = 1/K. \quad (3.24)$$

It is convenient now to introduce a mathematical device for manipulating the average number of hydrogen ions. This device takes the form of a weak external potential $U(\mathbf{r})$ which is applied to the system, with the specific form $\xi N_+(\mathbf{r})$. ξ is a small coupling constant. Obviously this external potential is constant across each of the regions $\Omega(N_+)$, but possesses discontinuities of integer multiples of ξ at their boundaries.

In the presence of the external potential, Eq. (3.22) obviously generalizes to the following:

$$P(N_+, \xi) = \left\{\int_{\Omega(N_+)} d\mathbf{r} \exp[-\beta\Phi(\mathbf{r}) - \beta\xi N_+(\mathbf{r})]\right\} \Big/ \left\{\sum_{N_+=0}^{N} \int_{\Omega(N_+)} d\mathbf{r} \exp[-\beta\Phi(\mathbf{r}) - \beta\xi N_+(\mathbf{r})]\right\}. \quad (3.25)$$

The corresponding change in the Gaussian form (3.23) may easily be shown to be

$$P(N_+, \xi) = (K/2\pi)^{1/2} \exp[-\tfrac{1}{2}K(N_+ - \langle N_+\rangle_0 + \xi/K)^2], \quad (3.26)$$

where $\langle N_+\rangle_0$ denotes the average when $\xi = 0$. One immediately sees that

the (linear) effect of external potential $U(\mathbf{r})$ on $\langle N_+ \rangle$ will be

$$\langle N_+ \rangle = \langle N_+ \rangle_0 - (\xi/K). \tag{3.27}$$

The quantity K^{-1} is a susceptibility conjugate to external potential strength ξ. Comparing Eqs. (3.24) and (3.27), one reaches a familiar type of conclusion, namely, that large quadratic fluctuations go hand in hand with large susceptibility to external potential.

We note in passing that the dissociation susceptibility K^{-1} may be expressed in terms of the hydrogen-ion pair distribution function $\rho^{(0,2,0)}$. Specifically, one calculates

$$1/K = \langle N_+ \rangle + \int d\mathbf{s}_1 \int d\mathbf{s}_2 [\rho^{(0,2,0)}(\mathbf{s}_1, \mathbf{s}_2) - \rho^{(0,1,0)}(\mathbf{s}_1)\rho^{(0,1,0)}(\mathbf{s}_2)], \tag{3.28}$$

wherein the distribution functions are those appropriate for the infinite system-size limit.

Equation (3.27) shows how variation in the strength ξ of the external potential $U(\mathbf{r})$ permits one in principle to manipulate the ion concentration in the water sample. If ξ changes from one steady value to another, the degree of dissociation will shift to accommodate that change. The rate at which the system relaxes to the new point of equilibrium is determined by kinetics of the dissociation process and its reverse. We will examine that relaxation process carefully and by doing so will be able to deduce a molecular expression for the chemical reaction rates.

First we need to examine the phenomenological kinetics implied by the fundamental reaction with which this article was opened:

$$H_2O \underset{k_a}{\overset{k_d}{\rightleftharpoons}} H^+ + OH^-. \tag{1.1}$$

The first-order rate equation implied by (1.1) is

$$\frac{d}{dt}\frac{\langle N_+ \rangle}{V} = k_d\left(\frac{N - \langle N_+ \rangle}{V}\right) - k_a\left(\frac{\langle N_+ \rangle}{V}\right)^2. \tag{3.29}$$

Equation (3.27) shows that the final change in hydrogen-ion concentration caused by a sudden small change $\delta\xi$ in external potential will be $-\delta\xi/VK$; kinetic equation (3.29) requires that the approach to this change will be exponential in time. If the cited change $\delta\xi$ occurs at time t_0, the subsequent change in hydrogen ion concentration will be given by

$$\delta\left(\frac{\langle N_+ \rangle}{V}\right) = \frac{\delta\xi}{VK}\{\exp[-k_r(t - t_0)] - 1\} \qquad (t \geq t_0). \tag{3.30}$$

In this expression, the relaxation rate k_r is

$$k_r = k_d + 2(\langle N_+ \rangle_0/V)k_a. \tag{3.31}$$

The response to any small, but otherwise arbitrary, time-varying ξ may easily be synthesized from exponential lags of type (3.30). By invoking linearity of response, one obtains the general phenomenological result:

$$\frac{d}{dt}\frac{\langle N_+ \rangle}{V} = -\frac{k_r}{VK}\int_{-\infty}^{t} ds \exp[-k_r(t-s)]\frac{d\xi(s)}{ds}. \tag{3.32}$$

In studying relaxation processes such as this it is important to observe response to perturbations of different frequencies, so we can set

$$\xi(t) = \xi_0 \exp(i\omega t), \tag{3.33}$$

where ω must have a negative imaginary part to ensure convergence. Insert this $\xi(t)$ into Eq. (3.32) to find

$$\frac{d}{dt}\frac{\langle N_+ \rangle}{V} = -\frac{i\omega\xi_0 k_r \exp(i\omega t)}{VK(k_r + i\omega)}. \tag{3.34}$$

This is the phenomenological expression whose comparison with microscopic theory generates a new expression for k_r.

Chronological evolution of the system of $3N$ nuclei may be described by the phase space probability function $f(\mathbf{r}, \mathbf{p}, t)$. This function satisfies the Liouville equation

$$\partial f/\partial t = i\mathscr{L}(t)f; \tag{3.35}$$

$\mathscr{L}$ is the Liouville operator

$$\mathscr{L}(t) = i\sum_{j=1}^{3N}\left[\frac{1}{m_j}\mathbf{p}_j \cdot \nabla_{\mathbf{r}_j} + \mathbf{F}_j(t) \cdot \nabla_{\mathbf{p}_j}\right]. \tag{3.36}$$

The force $\mathbf{F}_j(t)$ acting on nucleus j consists of two parts. The first, $\mathbf{F}_j^{(0)}$, is due simply to internal forces within the system (including wall forces):

$$\mathbf{F}_j^{(0)} = -\nabla_{\mathbf{r}_j}\Phi, \tag{3.37}$$

and has no explicit dependence on time t. The other part, $\mathbf{F}_j^{(1)}(t)$, is the external force on nucleus j due to $U = \xi N_+$:

$$\mathbf{F}_j^{(1)}(t) = -\xi_0 \exp(i\omega t)\nabla_{\mathbf{r}_j} N_+(\mathbf{r}). \tag{3.38}$$

Notice that these latter forces act impulsively; in the $9N$-dimensional configuration space the vector $\nabla N_+(r)$ vanishes except at the boundaries of the region $\Omega(N_+)$, and at these boundaries it has normal orientation from smaller to larger N_+.

We can split the Liouville operator $\mathscr{L}$ into an unperturbed part $\mathscr{L}_0$, and the equilibrium-shifting perturbation $\mathscr{L}_1(t)$:

$$\mathscr{L}(t) = \mathscr{L}_0 + \mathscr{L}_1(t),$$

$$\mathscr{L}_1(t) = i\sum_{j=1}^{3N}\mathbf{F}_j^{(1)}(t) \cdot \nabla_{\mathbf{p}_j}. \tag{3.39}$$

Under the assumption that f was the equilibrium distribution function f_{eq} in the remote past, and that subsequently $\mathscr{L}_1(t)$ was sufficiently weak that only linear response need be considered, then the perturbed distribution function at time t may be displayed in the following form:

$$f(\mathbf{r}, \mathbf{p}, \mathbf{t}) = f_{eq}(\mathbf{r}, \mathbf{p}) - \xi_0 \beta \int_{-\infty}^{t} ds \exp[i(t-s)\mathscr{L}_0] \times \exp(i\omega s) f_{eq}(\mathbf{r}', \mathbf{p}') \sum_{j=1}^{3N} \nabla_{\mathbf{r}_j} N_+(\mathbf{r}') \cdot (\mathbf{p}_j'/m_j). \quad (3.40)$$

Here $\mathbf{r}'$, $\mathbf{p}'$ stand for phase-space coordinates which unperturbed motion over interval $t - s$ carries into $\mathbf{r}$, $\mathbf{p}$. The quantity

$$J_+(\mathbf{r}, \mathbf{p}) = \sum_{j=1}^{3N} \nabla_{\mathbf{r}_j} N_+(\mathbf{r}) \cdot (\mathbf{p}_j/m) \quad (3.41)$$

represents the total normal current (in the increasing N_+ direction) crossing the Ω boundaries in the $9N$-dimensional configuration space. Hence we can write for the linear approximation:

$$f(\mathbf{r}, \mathbf{p}, t) = f_{eq}(\mathbf{r}, \mathbf{p}) - \xi_0 \beta \int_{-\infty}^{t} ds \exp(i\omega s) J_+(\mathbf{r}', \mathbf{p}') f_{eq}(\mathbf{r}', \mathbf{p}'). \quad (3.42)$$

The expected rate of change of N_+ at time t likewise can be expressed in terms of the current J_+:

$$\frac{d\langle N_+(t)\rangle}{dt} = \int d\mathbf{r} \int d\mathbf{p} f(\mathbf{r}, \mathbf{p}, t) J_+(\mathbf{r}, \mathbf{p}). \quad (3.43)$$

Of course f_{eq} produces no average rate of change for N_+, but the perturbed part of f does. Using expression (3.42) in Eq. (3.43), one finds

$$\frac{d}{dt}\frac{\langle N_+(t)\rangle}{V} = -\frac{\xi_0 \beta}{V} \int d\mathbf{r} \int d\mathbf{p} \int_{-\infty}^{t} ds \exp(i\omega s) \times J_+(\mathbf{r}, \mathbf{p}) J_+(\mathbf{r}', \mathbf{p}') f_{eq}(\mathbf{r}', \mathbf{p}'), \quad (3.44)$$

or more succinctly,

$$\frac{d}{dt}\frac{\langle N_+\rangle}{V} = -\frac{\xi_0 \beta}{V} \exp(i\omega t) \int_{-\infty}^{0} ds \langle J_+(0) J_+(s)\rangle \exp(i\omega s), \quad (3.45)$$

where $\langle \cdots \rangle$ represents an average taken at equilibrium.

At least within the regime of classical dynamics, Eq. (3.45) represents the exact linear response to the arbitrary-frequency perturbation $\xi(t)N_+(\mathbf{r})$ that we have used to disturb the equilibrium. It must now be compared to the

phenomenological expression (3.34). Owing to the elementary stochastic assumptions upon which (3.34) is based, we cannot possibly expect the two expressions to agree precisely. In particular, the full molecular dynamics involves detailed high-frequency motions (e.g., vibrations and librations) that play no explicit part in phenomenological chemical kinetics. Nevertheless we can demand agreement between Eqs. (3.34) and (3.45) for small ω. This can be accomplished by expanding both in formal power series in ω, and demanding equality in corresponding orders. In fact it is consistent to make this demand only in the first three orders, and upon doing so one obtains the three relations:

$$\begin{aligned} &\int_{-\infty}^{0} ds\, \langle J_+(0)J_+(s)\rangle = 0, \\ &\int_{-\infty}^{0} ds\, s\langle J_+(0)J_+(s)\rangle = 1/K\beta, \\ &\int_{-\infty}^{0} ds\, s^2\langle J_+(0)J_+(s)\rangle = -(2/\beta K k_r). \end{aligned} \tag{3.46}$$

Consequently we have a microscopic expression for the chemical equilibrium relaxation time k_r^{-1} strictly in terms of current autocorrelation function integrals:

$$\frac{1}{k_r} = \left[\int_0^{\infty} ds\, s^2\langle J_+(0)J_+(s)\rangle\right] \Big/ \left[2\int_0^{\infty} ds\, s\langle J_+(0)J_+(s)\rangle\right]. \tag{3.47}$$

Here we have used the fact that the current autocorrelation average must be an even function of s, because of dynamical reversibility. Equation (3.47) is the major result of this section.

It may be of some pedagogic interest to inquire what form the current autocorrelation function would need to be in order to give the phenomenological result (3.34) exactly. In other words,

$$\frac{i\omega k_r}{K(k_r + i\omega)} \equiv \beta \int_{-\infty}^{0} ds\, \langle J_+(0)J_+(s)\rangle \exp(i\omega s). \tag{3.48}$$

The one-sided Fourier transform may easily be inverted to find

$$\langle J_+(0)J_+(s)\rangle = (2k_r/\beta K)\,\delta(s) - (k_r^2/\beta K)\exp(-k_r|s|). \tag{3.49}$$

The meaning of these two terms is very simple. The first, with infinitesimal duration, represents thermally driven "noise" in N_+, associated with stochastic crossing of the $\Omega(N_+)$ boundaries in configuration space. These fluctuations create small deviations from the equilibrium value of N_+ appropriate for the prevailing temperature and pressure conditions. Consequently, relax-

ation back to equilibrium ensues, which is described by the second term in Eq. (3.49).

The exact autocorrelation function can be expected to differ in several important ways from the "model function" (3.49). Although the existence of discrete jumps in N_+ will necessarily give rise to a delta-function contribution proportional to absolute temperature, the corresponding multiplier is not given correctly by Eq. (3.49). Instead, the correct expression requires an integral over the entire set of $\Omega(N_+)$ boundaries.

Vibrational and librational motions can also be expected to cause deviations from form (3.49) at short (but nonzero) times. These oscillatory mo-

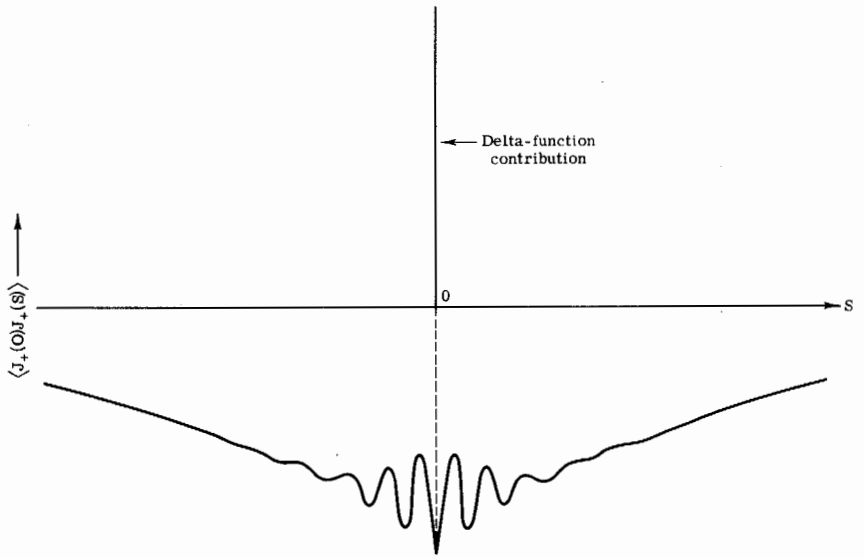

Fig. 11. Current autocorrelation function for the chemical relaxation rate in Eq. (3.47). This is only a schematic representation.

tions will frequently cause the boundaries in configuration space to be crossed back and forth in rapid succession. This will tend to give a strongly negative bias to the autocorrelation at very small times, followed by damped oscillations. The qualitative appearance of $\langle J_+(0)J_+(s)\rangle$ is shown in Fig. 11.

If we were dealing with a slow relaxation process, much slower than vibrational and librational periods in the liquid, then it is plausible that the long-time autocorrelation behavior of J_+ would be nearly a single exponential. However the association–dissociation relaxation in pure water is inherently so fast that such a clean separation of time scales does not always

obtain. In particular, one might find important departures from exponential behavior in hot compressed water where the equilibrium ion concentration is high. However, in water at 25°C at 1 atm, the measured relaxation time k_r^{-1} is 3.5×10^{-5} seconds (Eigen and DeMaeyer, 1958), which should indeed lead to nearly exponential behavior over most of the correlation time.

Debye has developed a theory for reaction rates between ionic species in solution (Debye, 1942). With suitable reinterpretation, this theory provides a description of the neutralization reaction between H^+ and OH^- in water, i.e., a description of the processes which determine k_a in Eq. (1.1). The necessary reinterpretation has been advanced by Eigen and DeMaeyer (1958). They conclude that the following expression is valid:

$$k_a = \frac{4\pi e^2}{\varepsilon_0 k_B T}\left[\frac{D_+ + D_-}{\exp(e^2/\varepsilon_0 a k_B T) - 1}\right]. \tag{3.50}$$

Here D_+ and D_- are the apparent self-diffusion constants for the ions, and a is a "reaction distance" such that one assumes that whenever an H^+ and OH^- approach each other this closely they inevitably and quickly react. Using experimental values for k_a, ε_0, and ion mobilities at room temperature, Eigen and DeMaeyer conclude that

$$a = 7.5 \pm 2 \text{ Å}. \tag{3.51}$$

This distance should probably be interpreted as the point of contact between ion solvation regions containing foreshortened hydrogen bonds. Considering the polarization of respective H^+ and OH^- containing regions, such contact would produce a complete chain of such short bonds along which immediate charge transport would occur to produce the neutralization reaction. In this way, Eq. (3.50) provides an important link to the quantum-mechanical (and crystallographic) studies of H^+ and OH^- solvation structures.

This last result is also important in achieving the proper interpretation of the general rate constant expression (3.47). In particular, it suggests that the type of hypersurface crossing illustrated in Fig. 9 (involving formal hopping of H^+ simultaneously over several molecules) may indeed be quite important in water. By dynamical reversibility, the spontaneous dissociation reaction must also involve sudden charge separation by at least distance a, which likewise may frequently proceed by the concerted process of Fig. 9.

Providing that a suitable Hamiltonian model can be constructed to describe dissociating water, the molecular dynamics simulation technique could offer basic insights into the relative contributions to the various types of hypersurface crossings to the reaction rates.

D. Quantum-Mechanical Extension

Just as it was necessary earlier to indicate how molecular distribution functions must be calculated in the quantum-mechanical regime, so too must we examine the corresponding changes for the theory of reaction rates. In a convenient review article, Zwanzig has stated the general relationship between classical and quantum-mechanical expressions for transport and rate constants in current correlation function form (Zwanzig, 1965). This, of course, is the form in which the relaxation rate k_r has been displayed in Eq. (3.47) above. Consequently we can immediately adapt Zwanzig's exposition to the water problem.

The quantum-mechanical extension requires first that the currents J_+ appearing in Eq. (3.47) be replaced by the appropriate operators, and then that the thermal average $\langle \cdots \rangle$ be carried out as a trace with the quantum-mechanical density matrix for the system, $\exp(-\beta \mathscr{H})$.

First note that in the classical regime,

$$J_+(t) = (d/dt)N_+(t); \tag{3.52}$$

$N_+(t)$ is the number of H^+ ions in the system defined by the algorithm stated earlier. We associate with N_+ the quantum-mechanical operator $\mathscr{N}_+$ which, in the position representation, multiplies any given wave function for the system by the appropriate number N_+ for the configuration of interest. The time derivative of $\mathscr{N}_+$ satisfies Heisenberg's equation of motion:

$$\dot{\mathscr{N}}_+ = (i/\hbar)[\mathscr{H}, \mathscr{N}_+], \tag{3.53}$$

where [,] stands for the commutator. The formal solution to Eq. (3.53) is

$$\mathscr{N}_+(t) = \exp(it\mathscr{H}/\hbar)\,\mathscr{N}_+(0)\exp(-it\mathscr{H}/\hbar). \tag{3.54}$$

In order to display the correct quantum-mechanical generalization, one must use the "Kubo transform" $\dot{\mathscr{N}}_+^{(K)}(t)$ for the operator $\dot{\mathscr{N}}_+(t)$:

$$\dot{\mathscr{N}}_+^{(K)}(t) = \beta^{-1}\int_0^\beta d\lambda \exp(\lambda\mathscr{H})\dot{\mathscr{N}}_+(t)\exp(-\lambda\mathscr{H}). \tag{3.55}$$

We thus have the following quantum version of Eq. (3.47):

$$\frac{1}{k_r} = \left[\int_0^\infty ds\, s^2\langle \dot{\mathscr{N}}_+^{(K)}(0)\dot{\mathscr{N}}_+(s)\rangle\right] \Big/ \left[\int_0^\infty ds\, s\langle \dot{\mathscr{N}}_+^{(K)}(0)\dot{\mathscr{N}}_+(s)\rangle\right]. \tag{3.56}$$

This last result should be central in any discussion of kinetic isotope effects on the association–dissociation relaxation in water. In some small degree, the isotopic difference in structure between H_2O and D_2O would affect this relaxation rate. But more important probably are (1) the relative rates of network restructuring, and (2) the influence of tunnelling on H^+ or

D^+ motion. The first of these can roughly be correlated with comparison of dielectric relaxation times and self-diffusion constants for H_2O and D_2O (see Table III). The second should be reflected in a diminished a value for D_2O compared to H_2O, when the Debye equation (3.50) is used to infer an effective reaction distance.

An obvious need exists at present to measure relaxation rates and ion mobilities accurately in D_2O over an extended density and temperature range, to permit quantitative comparison with the corresponding H_2O results. The comparison should help to assess the magnitude of quantum corrections to kinetic properties in liquid water.

E. Reactions Involving Other Species

The association–dissociation reaction (1.1), of course, is always present in water, even when it acts as a host solvent for other chemical reactions. If these latter reactions themselves involve H^+ or OH^-, there arises a strong coupling between solvent and solute reactions. We shall illustrate the way that theory describes this coupling by examining the specific case of acid dissociation in water. This example serves to clarify concepts required for describing other aqueous reactions of the type mentioned in Section I,D.

The competing reactions to be considered involve four phenomenological rate constants:

$$\begin{aligned} &H_2O \underset{k_a}{\overset{k_d}{\rightleftharpoons}} H^+ + OH^- \\ &HA \underset{K_a}{\overset{K_d}{\rightleftharpoons}} H^+ + A^-. \end{aligned} \tag{3.57}$$

In the dilute solution limit k_a and k_d may, of course, be taken as the rates appropriate for pure water, but in general k_a, k_d, K_a, and K_d will depend upon composition of the binary solution.

First we need to know the relaxation spectrum implied by Eqs. (3.57) for sufficiently small deviations from equilibrium that time-dependent composition variations of $k_a \cdots K_a$ may be neglected. Let $C_0(v)$ denote the equilibrium concentration of species v. Starting from some initial state of disturbed equilibrium, we can represent the time-dependent concentrations of the five species as follows:

$$\begin{aligned} H_2O &: C_0(H_2O) - x(t) \\ HA &: C_0(HA) - y(t) \\ OH^- &: C_0(OH^-) + x(t) \\ A^- &: C_0(A^-) + y(t) \\ H^+ &: C_0(H^+) + x(t) + y(t). \end{aligned} \tag{3.58}$$

The corresponding linear first-order differential equations are easily found to be

$$-\dot{x}(t) = k_d x + k_a[C_0(H^+) + C_0(OH^-)]x + k_a C_0(OH^-)y,$$
$$-\dot{y}(t) = K_d y + K_a[C_0(H^+) + C_0(A^-)]y + K_a C_0(A^-)x. \tag{3.59}$$

The general solution to Eqs. (3.59) consists of linear combinations of two exponentially decaying function pairs of the type

$$x(t) = \exp(-\alpha t),$$
$$y(t) = y(0)\exp(-\alpha t). \tag{3.60}$$

Substituting this form into Eqs. (3.59) yields

$$y(0) = \frac{K_a C_0(A^-)}{\alpha - S}, \tag{3.61}$$

and

$$\alpha^2 - (s + S)\alpha + sS - k_a K_a C_0(OH^-)C_0(A^-) = 0, \tag{3.62}$$

where

$$s = k_d + k_a[C_0(H^+) + C_0(OH^-)],$$
$$S = K_d + K_a[C_0(H^+) + C_0(A^-)]. \tag{3.63}$$

Were it not for the last term in the left member of Eq. (3.62), the roots for the decay constant α would be precisely s and S. However, this last term, since it is negative, causes the upper root to rise above $\max(s, S)$ and the lower root to sink below $\min(s, S)$.

$$\alpha_\pm = \tfrac{1}{2}\{s + S \pm [(s - S)^2 + 4k_a K_a C_0(OH^-)C_0(A^-)]^{1/2}\}. \tag{3.64}$$

Although conditions in the binary solution may be such that $s = S$, notice that the two roots α_+ and α_- always remain distinct. For the larger root, $y(0)$ is positive, and this more rapid of the two relaxation modes has the water and the acid associating (or dissociating) together. The slower relaxation mode has negative $y(0)$, so one of the molecular constituents associates while the other dissociates.

In order to establish contact between the phenomenological equations (3.57) and the microscopic theory, we must once again articulate a procedure for dividing configuration space into regions that correspond to fixed numbers of the five chemical species. Obviously, we want the procedure to reduce to that already advocated for pure water when the constituent HA has zero concentration. Indeed, we shall follow the same bonding algorithm as before, after introducing a suitable prescription for formation of the H–A molecular bond.

In general, the geometric criterion of when an A^- particle and an available H^+ ought properly to be considered bonded should rest upon the nature of the relevant potential energy surface. If A^- were monoatomic (i.e., a halide anion), the spherical symmetry demands that a critical bond formation radius L' be identified [analogous to L for water, Eq. (3.1)]. This radius might best be defined as the outer surface at which the adiabatic H–A potential energy displays some fixed fraction, say one-half, of the maximum possible bond energy. For polyatomic anions, of course, the resulting binding criterion would have to be more complicated. Thus for a long-chain fatty acid, the criterion must assure that the bound proton resides in an appropriate region at the carboxylate end of the molecule. Tautomeric substances such as acetylacetone ($CH_3COCH_2COCH_3$) will in fact exhibit disconnected regions for H^+ attachment.

Assume now that the bonding criterion for H–A has been established. The algorithm for identifying H_2O, HA, OH^-, A^-, and H^+ particles in the solution, given the full set of nuclear coordinates, must proceed as follows.

1. Form a list of all distances between hydrogen nuclei and base-atom nuclei (O for water, and whatever atom or atoms act as points of H^+ attachment in HA). Arrange these distances in ascending order. Coincidental equalities have vanishing probability and may be disregarded.
2. Eliminate all distances that exceed the maximum permissible bond lengths either for water (L) or HA(L').
3. Bond the two nuclei that provide the minimum distance in the remaining list (in the case of HA we additionally may demand that angular requirements be met as well).
4. Remove from the list all distances that involve hydrogens previously bonded and/or involve base atoms bonded the maximum permissible number of times previously (twice for water oxygens, once for base atoms in A^-).
5. Proceed to the next larger distance remaining in the list, and bond the two nuclei involved if appropriate.

By processing the entire list of distances this way the hydrogens are at least partially assigned to the oxygen and A^- particles so as to identify uniquely H_2O and HA molecules, and OH^-, A^-, and H^+ ions. Notice that no hydrogen can simultaneously serve as part of more than just a single H_2O, HA, or OH^- entity. [This procedure consistently neglects hydrogens that may be part of the stable (nonexchangeable) structure of A^-; in the case of some tautomeric substances this simplifying assumption may require revision.]

The binary aqueous solution under consideration may be regarded as having originally been prepared from a fixed number N_{I} of undissociated water molecules mixed together with N_{II} originally undissociated HA molecules. After mixing, there will be fluctuating numbers $N_{\mathrm{w}}(t)$, $N_{\mathrm{HA}}(t)$,

$N_{OH}(t)$, $N_A(t)$, and $N_+(t)$ of the species H_2O, HA, OH^-, A^-, and H^+, respectively. The fluctuations represent only two statistical degrees of freedom, since we have the conservation conditions

$$\begin{aligned} N_w(t) + N_{OH}(t) &= N_I, \\ N_{HA}(t) + N_A(t) &= N_{II}, \\ N_{OH}(t) + N_A(t) &= N_+(t). \end{aligned} \tag{3.65}$$

The anion numbers N_{OH} and N_A offer a convenient pair of independent variables. These discrete variables completely partition the multidimensional configuration space for the system into distinct regions $\Omega(N_{OH}, N_A)$ that yield the indicated numbers of particles through the stated bonding algorithm.

Next we must calculate the linear response of the system to application of a weak external perturbation potential of the type

$$U(\mathbf{r}, t) = [\xi_0 N_{OH}(\mathbf{r}) + \xi_1 N_A(\mathbf{r})] \exp(i\omega t). \tag{3.66}$$

Here ξ_0 and ξ_1 are small constants, possibly complex. The frequency ω should be given a small negative imaginary part to ensure convergence. Obviously U is constant across each region $\Omega(N_{OH}, N_A)$.

As was the case with pure water, the linear response may be computed from the Liouville equation, assuming that classical mechanics applies. This response may be expressed in terms of correlation functions of currents:

$$J_{OH} = dN_{OH}/dt, \qquad J_A = dN_A/dt,$$

which measure crossings of $\Omega(N_{OH}, N_A)$ boundaries. There is no need to reproduce the derivation, which merely parallels that of the earlier case. One obtains the following results:

$$\begin{aligned} \frac{d}{dt}\frac{\langle N_{OH}(t)\rangle}{V} &= -\frac{\beta \exp(i\omega t)}{V}[\xi_0 \Phi_1(\omega) + \xi_1 \Phi_3(\omega)], \\ \frac{d}{dt}\frac{\langle N_A(t)\rangle}{V} &= -\frac{\beta \exp(i\omega t)}{V}[\xi_1 \Phi_2(\omega) + \xi_0 \Phi_3(\omega)], \end{aligned} \tag{3.67}$$

where

$$\begin{aligned} \Phi_1(\omega) &= \int_0^\infty ds \exp(-i\omega s)\langle J_{OH}(0) J_{OH}(s)\rangle, \\ \Phi_2(\omega) &= \int_0^\infty ds \exp(-i\omega s)\langle J_A(0) J_A(s)\rangle, \\ \Phi_3(\omega) &= \int_0^\infty ds \exp(-i\omega s)\langle J_{OH}(0) J_A(s)\rangle. \end{aligned} \tag{3.68}$$

There will exist two characteristic values of the ratio ξ_1/ξ_0, each of which will induce a value for the response ratio $\langle \dot{N}_A(t)\rangle/\langle \dot{N}_{OH}(t)\rangle$ numerically equal to that ξ_1/ξ_0 ratio itself. From Eqs. (3.67) one easily finds that these characteristic ratios are

$$\frac{\xi_1}{\xi_0} = R_\pm = \frac{1}{2\Phi_3}\{\Phi_2 - \Phi_1 \pm [(\Phi_2 - \Phi_1)^2 + 4(\Phi_3)^2]^{1/2}\}. \tag{3.69}$$

Of course R_+ and R_- in principle depend on ω, but they should approach limiting values as $\omega \to 0$, with leading-order corrections that are quadratic in ω.

Consider now the case of small ω, and suppose ξ_1/ξ_0 in $U(\mathbf{r}, t)$ is chosen to be one of the values $R_\pm(0)$. Then the system responds by slowly shifting its equilibrium to accommodate the slowly varying external field. The extent to which the system can follow the field depends on the relaxation time involved, and one such time belongs to each of R_+ and R_-. These relaxation times must be identified with the phenomenological times $\alpha_\pm^{-1}$, from Eq. (3.64). It is clear, furthermore, that the $R_\pm(0)$ should be identified with the coefficient $y(0)$ in Eq. (3.60).

To state the situation in other terms, the two linear combinations of concentration fluctuations

$$\left(\frac{\Delta N_{OH}}{V}\right) + R_\pm\left(\frac{\Delta N_A}{V}\right) \tag{3.70}$$

are just those that should exhibit single relaxation behavior. The corresponding combination of Eqs. (3.67),

$$\frac{d}{dt}\frac{\langle N_{OH}\rangle + R_\pm\langle N_A\rangle}{V} = -\frac{\beta \exp(i\omega t)\xi_0}{V}\{\Phi_1(\omega) + 2R_\pm\Phi_3(\omega) + R_\pm^2\Phi_2(\omega)\} \tag{3.71}$$

should therefore manifest a right member with ω dependence close to that for simple relaxation behavior ($K_\pm > 0$):

$$\frac{-i\omega\alpha_\pm}{K_\pm(\alpha_\pm + i\omega)}\left[\frac{\xi_0 \exp(i\omega t)}{V}\right]. \tag{3.72}$$

In order to produce expressions for the relaxation times in terms of current correlation functions, it is necessary to expand both (3.71) and (3.72) through quadratic order in ω, and then compare corresponding terms. To the extent that separate relaxation times are indeed identifiable, ω dependence of $R_\pm$ should be negligible. Under that assumption we find the follow-

ing molecular expressions for the chemical relaxation times:

$$\alpha_{\pm}^{-1} = \frac{\Phi_1^{(2)} + 2R_{\pm}(0)\Phi_3^{(2)} + R_{\pm}^2(0)\Phi_2^{(2)}}{2[\Phi_1^{(1)} + 2R_{\pm}(0)\Phi_3^{(1)} + R_{\pm}^2(0)\Phi_2^{(1)}}; \tag{3.73}$$

we have introduced the correlation function moment quantities

$$\Phi_1^{(n)} = \int_0^\infty ds\, s^n \langle J_{OH}(0) J_{OH}(s)\rangle,$$

$$\Phi_2^{(n)} = \int_0^\infty ds\, s^n \langle J_A(0) J_A(s)\rangle,$$

$$\Phi_3^{(n)} = \int_0^\infty ds\, s^n \langle J_{OH}(0) J_A(s)\rangle. \tag{3.74}$$

The procedure outlined in Section III,D can readily be adapted to provide the quantum-mechanical version of expression (3.73).

If the molecular dynamics described by Eqs. (3.67) were precisely characteristic of a two-relaxation-process situation, then each of the Fourier transforms $\Phi_1(\omega)$, $\Phi_2(\omega)$, and $\Phi_3(\omega)$ would possess simple poles in the complex ω plane at $i\alpha_+$ and $i\alpha_-$. As we shall see in Section IV, however, this simple meromorphic character may not actually apply to the real aqueous solution case. Consequently, it is safer to rely on moment equations such as (3.73) to identify chemical relaxation rates.

It is important to keep in mind that rate coupling between the reactions (3.57) does not occur merely because both involve the same constituent H^+. The presence of HA and/or A^- in high concentration generally will affect the hydrogen-bond connectivity of the water network, and that in turn will affect the ability of the network to transport protons.

IV. Electrical Response

A. Frequency-Dependent Dielectric Function

Consider a region of empty space, for example that between parallel capacitor plates, which has an electrical field $\mathbf{E}_{ap}$ varying harmonically with time:

$$\mathbf{E}_{ap}(t) = \mathbf{E}_0 \exp(i\omega t). \tag{4.1}$$

If the region is then filled with homogeneous and isotropic matter (such as water or an aqueous solution), that matter then develops a polarization $\mathbf{P}$ which, in the linear response regime, may be related to $\mathbf{E}_{ap}$ through the

frequency-dependent dielectric function $\varepsilon(\omega)$:

$$4\pi\mathbf{P}(t) = \left[1 - \frac{1}{\varepsilon(\omega)}\right]\mathbf{E}_{ap}(t). \tag{4.2}$$

This polarization density causes the actual mean electrical field in the sample to be

$$\mathbf{E}(t) = \mathbf{E}_{ap}(t)/\varepsilon(\omega). \tag{4.3}$$

In general $\varepsilon(\omega)$ will be complex, and conventionally it is written in the following form:

$$\varepsilon(\omega) = \varepsilon'(\omega) - i\varepsilon''(\omega). \tag{4.4}$$

The imaginary part $-\varepsilon''$ represents dissipation. At very low frequency the dissipation in water and its solutions will be due to electrical conduction; this conductivity causes ε'' to diverge at $\omega = 0$:

$$\varepsilon''(\omega) = (4\pi\sigma/\omega) + 0(1), \tag{4.5}$$

where σ is the (low frequency) conductivity. As ω increases, absorbing regions of frequency are encountered which correspond in turn to molecular rotational relaxation ($\approx 10\ \text{cm}^{-1}$), to vibrational relaxation ($\approx 10^3\ \text{cm}^{-1}$), and finally to electronic excitation ($\approx 10^5\ \text{cm}^{-1}$).

The real and imaginary parts of $\varepsilon(\omega)$ are not independent, but are related to each other by the Kramers–Kronig equations (Kittel, 1958):

$$\varepsilon'(\omega) - \varepsilon'(\infty) = \frac{2}{\pi}\int_0^\infty \frac{u\varepsilon''(u)}{u^2 - \omega^2}\,du, \tag{4.6}$$

$$\varepsilon''(\omega) = -\frac{2\omega}{\pi}\int_0^\infty \frac{\varepsilon'(u) - \varepsilon'(\infty)}{u^2 - \omega^2}\,du. \tag{4.7}$$

Cauchy principal values for these integrals are to be taken at the integrand singularities. These Kramers–Kronig relations are simply a mathematical statement of causality, following from the requirement that medium response not precede the external perturbation.

The conductivity pole in ε'' at $\omega = 0$, shown in Eq. (4.5), necessarily affects ε' through Eq. (4.6). One easily demonstrates that near $\omega = 0$, ε' has to diverge to infinity as well. This merely reflects the ability of a conductor to shield completely any static electric field impressed upon it. However, pure water at least is a rather poor conductor ($0.04 \times 10^{-6}\ \Omega^{-1}\ \text{cm}^{-1}$ at 18°C), and so a convenient range of relatively low frequencies ($\approx 10^5$ Hz) is available over which a "static dielectric constant" ε_0 can experimentally be identified (as an attribute of water as a polar liquid consisting essentially of intact molecules) without significant interference from conductivity.

A satisfactory, completely general, theory of $\varepsilon(\omega)$ does not exist, which accounts for molecular motions, interactions, and polarizability. However some insight into the time-dependent dielectric behavior of water is possible through the theory restricted to rigid polar (but nonpolarizable) molecules. In this latter regime, $\varepsilon(\omega)$ may be calculated according to the following formula (Titulaer and Deutch, 1974):

$$\frac{[\varepsilon(\omega)-1][2\varepsilon(\omega)+1]\varepsilon_0}{(\varepsilon_0-1)(2\varepsilon_0+1)\varepsilon(\omega)} = -\int_0^\infty dt\, \exp(-i\omega t)\frac{d\phi(t)}{dt}. \tag{4.8}$$

In this expression, $\phi(t)$ stands for the normalized autocorrelation function of the moment $\mathbf{m}$ of a microscopically large, but macroscopically small, sphere of the substance, embedded in an infinite sea of its own kind.

$$\phi(t) = \langle \mathbf{m}(0)\cdot\mathbf{m}(t)\rangle/\langle m^2\rangle. \tag{4.9}$$

The simplest reasonable form that one might expect for $\phi(t)$ is that for single exponential decay

$$\phi(t) = \exp(-t/\tau) \qquad (t \geq 0). \tag{4.10}$$

By inserting this form into Eq. (4.8) one concludes

$$\varepsilon(\omega) = \frac{2\varepsilon_0^2 + i\omega\tau\varepsilon_0 - 1 + [Q(\varepsilon_0,\omega)]^{1/2}}{4\varepsilon_0(1+i\omega\tau)},$$

$$Q(\varepsilon_0,\omega) = 4\varepsilon_0^4 + 4i\omega\tau\varepsilon_0^3 + (4 + 16i\omega\tau - 9\omega^2\tau^2)\varepsilon_0^2 - 2i\omega\tau\varepsilon_0 + 1. \tag{4.11}$$

Although this $\varepsilon(\omega)$ as a function of the complex variable ω is analytic in the neighborhood of the origin, it possesses characteristic singularities off the real axis. In particular, a simple pole resides at

$$\omega = i/\tau, \tag{4.12}$$

and a pair of square-root branch points exist at the roots of $Q(\varepsilon_0,\omega)$:

$$\omega = \frac{i}{9\varepsilon_0\tau}\{2\varepsilon_0^2 + 8\varepsilon_0 - 1 \pm 2[\varepsilon_0^4 + 8\varepsilon_0^3 + 6\varepsilon_0^2 - 13\varepsilon_0 - 2]^{1/2}\}. \tag{4.13}$$

Thus we see that a simple $\phi(t)$ can give rise to a relatively complicated dielectric function.

Expression (4.11) for $\varepsilon(\omega)$ should be compared with the elementary "single relaxation" form that is often quoted (Fröhlich, 1949):

$$\varepsilon(\omega) = \frac{\varepsilon_0 + i\omega\tau}{1+i\omega\tau}, \tag{4.14}$$

which exhibits only the simple pole at i/τ. Obviously Eq. (4.14) requires a more elaborate $\phi(t)$ than the one shown in Eq. (4.10).

Considerable theoretical interest has recently been devoted to "hydrodynamic tails" in correlation functions that determine transport and kinetic properties (Alder and Wainwright, 1970). In the case of angular momentum for a single molecule, local vorticity created by that molecule in its surroundings causes the autocorrelation function to display a $t^{-5/2}$ tail at long time t (Ailawadi and Berne, 1971). Likewise, the rank-one orientational correlation functions for a single molecule decay to zero at long time as $t^{-7/2}$ (Garisto and Kapral, 1974). We take these facts as evidence that $\phi(t)$ in Eq. (4.9) also should display a long-time inverse-power tail since, after all, the local moment $\mathbf{m}(t)$ is additively composed of separate molecular contributions. In particular, we would expect $t^{-7/2}$ to be the relevant behavior for $\phi(t)$. Then the Fourier transform quantity on the right side of the $\varepsilon(\omega)$ formula (4.8) would possess branch-point character at the origin of the complex ω plane, associated with occurrence of $\omega^{7/2}$ in a small-ω expansion. Evidently $\varepsilon(\omega)$ itself will have a branch point at $\omega = 0$.

Obviously liquid water as a dielectric substance is much more complicated than the assumptions behind Eq. (4.8) would permit. Nevertheless, the same features apply in water that cause one to conclude from Eq. (4.8) that $\varepsilon(\omega)$ contains a branch-point singularity at the origin. The resulting dielectric behavior is obviously relevant to the motion of ions in water, particularly H^+ and OH^-.

B. Electrical Conduction

The time-correlation function expression for the electrical conductivity σ has the following form (Zwanzig, 1965):

$$\sigma = \beta \int_0^\infty dt \langle J_x(0) J_x(t) \rangle. \tag{4.15}$$

J_x is the x-component of the total electrical current flowing in the system. This formula refers specifically to a system with unit volume subject to periodic boundary conditions. In the case of pure water, J_x obviously comprises contributions both from H^+ and OH^-; aqueous solutions may contain other charge carriers as well.

We have noted earlier that the high static dielectric constant ε_0 aids in production of carriers in water, owing to the negative solvation free energy of H^+ and OH^-. At the same time the frequency dependence in $\varepsilon(\omega)$ causes a retardation of the motion of these ions, since local polarization has difficulty in following ion drift. Temporal persistence of spontaneous current fluctuations at equilibrium is therefore damped somewhat, and the correlation

function expression (4.15) reflects that fact by yielding a correspondingly reduced σ value.

One special aspect of the dynamics of local polarization as it follows H^+ and OH^- motion is clear from Figs. 1 and 2. The sequential proton exchanges along hydrogen-bond chains (which produce high apparent mobilities) automatically switch the orientation of water molecules in a favorable way, without the necessity for real molecular rotation. The polarization lag that retards forward motion will therefore largely reside in regions to the side of the conductive chain.

In the case of a spherical ion of radius b moving through a fluid dielectric continuum, Zwanzig has calculated the dielectric friction (Zwanzig, 1970). His calculation assumed that the dielectric dispersion could be represented by a single relaxation time τ_d. The result for the dielectric friction constant ζ_d was the following:

$$\zeta_d = \frac{Kq^2(\varepsilon_0 - \varepsilon_\infty)\tau_d}{b^3\varepsilon_0(2\varepsilon_0 + 1)}. \tag{4.16}$$

Here q stands for the charge on the moving ion, and the constant K depends on the hydrodynamic boundary conditions applied at the surface of the ion:

$$\begin{aligned} K &= 3/8 \quad \text{(sticking)} \\ &= 3/4 \quad \text{(slipping)}. \end{aligned} \tag{4.17}$$

Although it may seem paradoxical that slipping conditions produce greater dielectric friction than sticking conditions, it should be realized that the former permits nearby liquid to flow faster around the moving ion, thereby creating a greater polarization lag.

Obviously, there are grave difficulties in attempting to apply Zwanzig's result (4.16) to H^+ or OH^- in water, because of the exchange character of motion for these ions. Furthermore, it is unclear what an appropriate choice for the radius b would be for these species. However the fact that ζ_d is essentially proportional to τ_d/ε_0 is suggestive, and perhaps not far from the truth for H^+ and OH^- in water. This ratio declines monotonically between 0° and 75°C by a factor of about 3.9. No doubt a substantial part of the rising mobilities (equivalent conductances) with increasing temperature of H^+ and OH^- shown in Table II can be attributed to this declining dielectric friction.

Another important ingredient in understanding temperature variations of H^+ and OH^- mobilities is the topological nature of hydrogen-bond connections between molecules, and the rate at which such connections break and reform in new patterns. Eigen's description of proton conduction and diffusion in water (Eigen, 1964) seems to demand the interpretation that the

liquid consists of disconnected finite (i.e., independent of system size) clusters of bonded water molecules, with stochastic repositioning of nearby water molecules to attach to the edge of a cluster acting as rate-determining events. However, recent molecular dynamics simulations (Geiger *et al.*, 1977) show instead that an extended space-filling network picture for liquid water is clearly preferable, when an energy definition of "hydrogen bond" is chosen which conforms to a wide range of other physical and chemical measurements and properties. To reconcile the apparent contradition, Eigen's hydrogen bonds would have to be restricted to greater binding energy and/or shorter O–O separation than required otherwise.

Figure 12 shows that even if the hydrogen bonds involved are strong

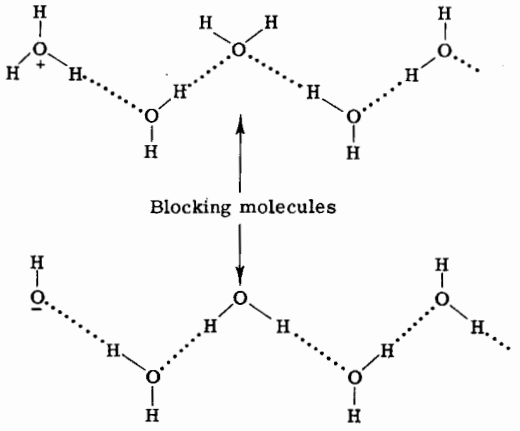

Fig. 12. Interrupted exchange pathways. Sequential proton jumps along a hydrogen-bond path for H^+ and OH^- transport can be blocked by a water molecule acting, respectively, as double proton acceptor (top) or double proton donor (bottom).

enough, a chain of bonds is not sufficient to guarantee the possibility of transport. All of these bonds must in fact be properly oriented beforehand. H^+ motion along a chain can effectively be blocked if a water molecule acting as a double proton acceptor is incorporated in that chain (Fig. 12, top). Likewise, a water molecule which acts as a double donor in a chain can effectively block passage of OH^- (Fig. 12, bottom). Evidently both formation and destruction of strong hydrogen bonds, as well as reorientations to shift "blocking molecules" are important in electrical conduction and ionic diffusion of H^+ and OH^- in water.

It is inherent in the crystallographic structure of ice that each molecule has many hydrogen bond paths passing through it. Considering any molecule and pairs of its four bonded neighbors, one sees that the chosen molecule simultaneously serves once as double proton donor, once as

double proton acceptor, and four times as a nonblocking molecule (Hankins *et al.*, 1970). The multiplicity of hydrogen-bond pathways in the crystal thus can permit blockages to be bypassed. Set against this topological advantage is the rigidity of the crystal that would inhibit formation of those very short and strong hydrogen bonds necessary for charge transport. Evidently, this latter feature dominates, for mobilities of H^+ and OH^- are less in ice than in liquid water, as noted earlier (Section I,B).

Owing to the relative magnitudes of three-molecule nonadditivity in water-molecule interactions, incorporation of "double donor" and "double acceptor" molecules in hydrogen bond chains is energetically unfavorable (Hankins *et al.*, 1970). Of these two, the double donor is the configuration more costly in energy. Unlike ice, the incompletely bonded liquid has a choice in how many blocking sites exist; therefore relatively fewer double donor occurrences than double acceptor occurrences are expected (the nonadditivity energy difference between them is approximately 0.5 kcal/mole.) Thus, blockage should more frequently occur for H^+ motion than for OH^- motion. Obviously, then, the fact exhibited in Table II that H^+ is more mobile than OH^- must stem from yet another feature; and indeed this feature must be sufficiently potent more than just to overcome the occurrence probabilities for blocking molecules.

The limiting equivalent conductances (Table II) imply the following activation energies for electrical charge transport at 20°C:

$$2.59 \text{ kcal/mole } (H^+),$$
$$3.11 \text{ kcal/mole } (OH^-). \tag{4.18}$$

It was stressed earlier in Sections II,B and C that hydrogen bonds in the immediate vicinity of a solvated H^+ tend to be stronger and shorter than those for a solvated OH^-. The difference in activation energies (4.18) indicates greater difficulty for OH^- compared to H^+ in reaching a "transition state" between successive "natural" configurations. One contributing factor to the difference is the presence of proton double minima for OH^- hydrogen bonds, in contrast to flat proton potentials for corresponding solvated H^+ structures. Another, and probably more important, factor is that solvated H^+ is surely surrounded on the average by a larger dendritic array of favorable hydrogen bonds than is solvated OH^-, owing to the tendency toward stronger bonds with the former. Consequently the H^+ hydration complex finds at its perimeter a greater set of configurational opportunities for easy proton transfer in the field direction and among this greater set will occur more opportunities for low-barrier transfers.

Notice that the ratio of mobilities of H^+ and OH^- tends toward unity as the temperature rises. Presumably this is associated with thermal disruption

of the respective solvation complexes. It would be useful to know by direct measurement if pressure rise has a similar effect.

We have noted that ionic motion in water is affected by coupling to dielectric dispersion, and that the frequency-dependent dielectric function $\varepsilon(\omega)$ exhibits branch-point characteristics in the complex ω plane. All chemical reactions in water involving proton transfer are therefore inevitably coupled to dielectric response and therefore partake of complex-ω branch-point behavior. This is the reason behind earlier cautioning (Section III,E) that the chemical current correlation transforms $\Phi_1(\omega)$, $\Phi_2(\omega)$, and $\Phi_3(\omega)$ in Eq. (3.68) should not cavalierly be treated as meromorphic functions.

C. Wien Effect

Wien was the first to point out that electrolytes display a characteristic non-Ohmic behavior; namely, their electrical conductance increases with increasing electrical field (Wien, 1928, 1931). This phenomenon exists for both strong and weak electrolytes. In the case of the former, the strong electrical field destroys the normal ion atmosphere, which exerts a retarding effect on ion mobility at small fields. In the case of the latter, strong fields enhance the rate of ionization without producing a compensating change in association rate. As a consequence, the weak electrolyte's ionization constant increases.

In comparison, the relative change in conductance at high fields is much greater for weak electrolytes than for strong electrolytes.

Onsager has worked out the theory of the Wien effect for weak electrolytes (Onsager, 1934). He concludes that the dissociation constant K_d should exhibit the following dependence on electric field strength E:

$$\frac{K_d(E)}{K_b(0)} = \frac{J_1[4(-\zeta_0 q)^{1/2}]}{2(-\zeta_0 q)^{1/2}}$$

$$= 1 + 2\zeta_0 q + \frac{(4\zeta_0 q)^2}{2!3!} + \frac{(4\zeta_0 q)^3}{3!4!} + \ldots, \tag{4.19}$$

where for a 1–1 electrolyte

$$q = \frac{e^2}{2\varepsilon_0 k_B T}, \qquad \zeta_0 = \frac{|eE|}{2k_B T}. \tag{4.20}$$

J_1 is the usual Bessel function which, for the imaginary argument shown, is monotonic. It is noteworthy that Onsager's result (4.19) depends on the absolute value of the field in such a way that the leading order effect is proportional to $|E|$ itself. In fact, that linear field effect would actually not apply at very small fields, owing to neglect of terms in derivation of Eq. (4.19). However, in the case of water, these neglected terms (associated

with ion atmosphere perturbation) are appreciable only at very small fields indeed.

With an electrical field of 100 kV/cm in water at 25°C, one has

$$q = 3.5790 \times 10^{-8} \text{ cm},$$

$$\zeta_0 = 1.9462 \times 10^{6} \text{ cm}^{-1},$$

$$K_d(E)/K_d(0) = 1.146, \tag{4.21}$$

which incorporates only slight deviation from Onsager's linear field effect regime.

Eigen and DeMaeyer have employed the Wien effect in pure water to study the rate of the fundamental recombination reaction (1.1) (Eigen and DeMaeyer, 1955). They used field strengths in the range 50–100 kV/cm, with rise times less than 10^{-8} sec to generate extra H^+ and OH^- ions in the liquid. The relaxation engendered by the subsequent neutralization reaction could then be monitored as electrical conductivity change.

V. Conclusions

The present exposition provides a formal theoretical framework for proton transfer reactions and kinetics in water. A major advantage of such a formalism is that it helps point out areas of incomplete information. Consequently, it seems highly desirable to pursue the following in the near future.

1. More detailed and accurate quantum-mechanical studies of potential energy surfaces for solvated H^+ and OH^- ions.
2. Monte Carlo and molecular dynamics investigation of H^+ and OH^- ions in water.
3. Experimental study of dielectric properties and H^+ and OH^- mobilities in supercooled water, and in water at elevated pressure.
4. Development of experimental techniques to study dissociation relaxation down to the picosecond range.
5. Measurement of dissociation relaxation in H_2O–D_2O mixtures.
6. Investigation of models for proton (and proton hole) transfer in random networks.

These projects, if successfully carried to completion, would substantially improve quantitative understanding of the subject of this review.

References

Ailawadi, N. K., and Berne, B. J. (1971). *J. Chem. Phys.* **54**, 3569–3571.
Alder, B. J., and Wainwright, T. E. (1970). *Phys. Rev. A.* **1**, 18–21.
Almlöf, J. (1972). *Acta Crystallogr., Sect. B* **28**, 481–485.
Almlöf, J., and Wahlgren, U. (1973). *Theor. Chim. Acta* **28**, 161–168.
Bell, R. A., Christoph, G. G., Fronczek, F. R., and Marsh, R. E. (1975). *Science* **190**, 151–152.
Benedict, W. S., Gailar, N., and Plyler, E. K. (1956). *J. Chem. Phys.* **24**, 1139–1165.
Bernal, J. D., and Fowler, R. H. (1933). *J. Chem. Phys.* **1**, 515–548.
Berry, R. S. (1969). *Chem. Rev.* **69**, 533–542.
Beurskens, G., and Jeffrey, G. A. (1964). *J. Chem. Phys.* **41**, 924–929.
Chamberlain, J. W., and Roesler, F. L. (1955). *Astrophys. J.* **121**, 541–547.
Chambers, R. D. (1973). "Fluorine in Organic Chemistry," p. 65. Wiley, New York.
Clough, S. A. (1976). Personal communication.
Collie, C. H., Hasted, J. B., and Ritson, D. M. (1948). *Proc. Phys. Soc. (London)* **60**, 145–160.
Covington, A. K., Robinson, R. A., and Bates, R. G. (1966). *J. Phys. Chem.* **70**, 3820–3824.
Darwent, B. deB. (1970). *Natl. Stand. Ref. Data Ser., Nat. Bur. Stand.* **31**, p. 41.
Debye, P. (1942). *Trans. Electrochem. Soc.* **82**, 265–271.
DePas, M., Leventhal, J. J., and Friedman, L. (1968). *J. Chem. Phys.* **49**, 5543–5544.
Dogonadze, R. R., Kharkats, Yu. I., and Ulstrup, J. (1976). *Chem. Phys. Lett.* **37**, 360–364.
Dyke, T. R., and Muenter, J. S. (1973). *J. Chem. Phys.* **59**, 3125–3127.
Eigen, M. (1964). *Angew. Chem.* **3**, 1–18.
Eigen, M., and DeMaeyer, L. (1955). *Z. Elektrochem.* **59**, 986–993.
Eigen, M., and DeMaeyer, L. (1958). *Proc. R. Soc. (London) Ser. A* **247**, 505–533.
Eisenberg, D., and Kauzmann, W. (1969). "The Structure and Properties of Water." Oxford Univ. Press, New York.
Fieser, L. F., and Fieser, M. (1956). "Organic Chemistry," p. 163. Reinhold, New York.
Finney, J. L. (1977). *Proc. R. Soc. (London) Ser. B* **278**, 3–31.
Fletcher, N. H. (1970). "The Chemical Physics of Ice." Cambridge Univ. Press, London and New York.
Fröhlich, H. (1949). "Theory of Dielectrics," p. 72. Oxford Univ. Press, London.
Garisto, F., and Kapral, R. (1974). *Phys. Rev. A.* **10**, 309–318.
Geiger, A., Rahman, A., and Stillinger, F. H. (1978). *J. Chem. Phys.*, to be published.
Grunwald, E., Loewenstein, A., and Meiboom, S. (1957). *J. Chem. Phys.* **27**, 630–640.
Hamann, S. D. (1963). *J. Phys. Chem.* **67**, 2233–2235.
Hankins, D., Moskowitz, J. W., and Stillinger, F. H. (1970). *J. Chem. Phys.* **53**, 4544–4554; Erratum (1973), **59**, 995.
Hepler, L. G., and Woolley, E. M. (1973). *In* "Water, A Comprehensive Treatise" (F. Franks, ed.), Vol. 3, p. 153. Plenum, New York.
Herzberg, G. (1950). "Molecular Spectra and Molecular Structure. I. Spectra of Diatomic Molecules," p. 560. Van Nostrand, Princeton, New Jersey.
Hill, T. L. (1956). "Statistical Mechanics." McGraw-Hill, New York.
Janoschek, R., Preuss, H., and Diercksen, G. (1967). *Int. J. Quantum Chem.* **1**, 649–652.
Jeffrey, G. A., Jordon, T. H., and McMullan, R. K. (1967). *Science* **155**, 689–691.
Jones, W. M. (1952). *J. Am. Chem. Soc.* **74**, 6065–6066.
Jones, W. M. (1968). *J. Chem. Phys.* **48**, 207–214.
Kebarle, P., Searles, S. K., Zolla, A., Scarborough, J., and Arshadi, M. (1967). *J. Am. Chem. Soc.* **89**, 6393–6399.
Kell, G. S., McLaurin, G. E., and Whalley, E. (1968). *J. Chem. Phys.* **49**, 2839–2842.

Kirkwood, J. G. (1939). *J. Chem. Phys.* 7, 911–919.
Kittel, C. (1958). "Elementary Statistical Physics," pp. 206–210. Wiley, New York.
Kollman, P. A., and Bender, C. F. (1973). *Chem. Phys. Lett.* **21**, 271–274.
Kotowski, A., ed. (1964). "Gmelins Handbuch der Anorganischen Chemie. Sauerstoff," Lieferung 6, System-Nummer 3, p. 1994. Verlag Chemie, Heidelberg.
Kraemer, W. P., and Diercksen, G. H. F. (1970). *Chem. Phys. Lett.* **5**, 463–465.
Kutz, H. D., Oppenheim, I., and Ben-Reuven, A. (1974). *J. Chem. Phys.* **61**, 3313–3326.
Lie, G. C., and Clementi, E. (1975). *J. Chem. Phys.* **62**, 2195–2199.
Long, F. A., and Purchase, M. (1950). *J. Am. Chem. Soc.* **72**, 3267–3273.
Long, F. A., Dunkle, F. B., and McDevit, W. F. (1951). *J. Phys. Colloid Chem.* **55**, 829–842.
Lundgren, J.-O. and Olovsson, I. (1967). *Acta Crystallogr.* **23**, 966–971, 971–976.
Lundgren, J.-O., and Olovsson, I. (1968). *J. Chem. Phys.* **49**, 1068–1074.
McMullan, R. K., Mak, T. C. W., and Jeffrey, G. A. (1966). *J. Chem. Phys.* **44**, 2338–2345.
Malmberg, C. G., and Maryott, A. A. (1956). *J. Res. Natl. Bur. Stand.* **56**, 1–8.
Mills, R. (1973). *J. Phys. Chem.* **77**, 685–688.
Narten, A. H. (1972). *J. Chem. Phys.* **56**, 5681–5687.
Narten, A. H., and Levy, H. A. (1971). *J. Chem. Phys.* **55**, 2263–2269.
Newton, M. D., and Ehrenson, S. (1971). *J. Am. Chem. Soc.* **93**, 4971–4990.
Olovsson, I. (1968). *J. Chem. Phys.* **49**, 1063–1067.
Onsager, L. (1934). *J. Chem. Phys.* **2**, 599–615.
Onsager, L. (1973). *In* "Physics and Chemistry of Ice" (E. Whalley, S. J. Jones, and L. W. Gold, eds.), p. 10. Royal Soc. of Canada, Ottawa.
Peterson, C., and Pfeiffer, G. V. (1972). *Theor. Chim. Acta* **26**, 321–330.
Popkie, H., Kistenmacher, H., and Clementi, E. (1973). *J. Chem. Phys.* **59**, 1325–1336.
Pople, J. A., Schneider, W. G., and Berstein, H. J. (1959). "High-Resolution Nuclear Magnetic Resonance," Chapter 18. McGraw-Hill, New York.
Rahman, A., and Stillinger, F. H. (1973). *J. Am. Chem. Soc.* **95**, 7943–7948.
Résibois, P. M. V. (1968). "Electrolyte Theory," p. 33. Harper, New York.
Robinson, R. A., and Stokes, R. H. (1959). "Electrolyte Solutions," p. 544, Butterworths, London.
Smith, D. F., and Overend, J. (1972). *Spectrochim. Acta* **28A**, 471–483.
Stillinger, F. H. (1975). *Adv. Chem. Phys.* **31**, 1–101.
Stillinger, F. H. (1977). *Proc. R. Soc. (London) Ser. B* **278**, 97–110.
Stillinger, F. H., and Lovett, R. (1968). *J. Chem. Phys.* **49**, 1991–1994.
Stillinger, F. H., and Rahman, A. (1974). *J. Chem. Phys.* **60**, 1545–1557.
Stoeckenius, W. (1976). *Sci. Am.* **234**, No. 6, 38–46.
Stokes, R. H., and Mills, R. (1965). *In* "International Encyclopedia of Physical Chemistry and Chemical Physics. Topic 16: Transport Properties of Electrolytes" (E. A. Guggenheim, J. E. Mayer, and F. C. Tompkins, eds.), Vol. 3, p. 74. Pergamon, New York.
Swalen, J. D., and Ibers, J. A. (1962). *J. Chem. Phys.* **36**, 1914–1918.
Titulaer, U. M., and Deutch, J. M. (1974). *J. Chem. Phys.* **60**, 1502–1513.
Tödheide, K. (1972). *In* "Water, A Comprehensive Treatise" (F. Franks, ed.), Vol. 1, pp. 463–513. Plenum, New York.
Van Raalte, D., and Harrison, A. G. (1963). *Can. J. Chem.* **41**, 3118–3126.
Vereschagin, L. F., Yakovlev, E. N., and Timofeev, Yu. A. (1975). *JETP Lett.* **21**, 304–305.
Vidulich, G. A., Evans, D. F., and Kay, R. L. (1967). *J. Phys. Chem.* **71**, 656–662.
Weast, R. C., ed. (1975). "Handbook of Chemistry and Physics," 56th edition, pp. D136–D139. Chemical Rubber Co., Cleveland, Ohio.
Wiberg, K. B. (1964). "Physical Organic Chemistry," p. 252. Wiley, New York.
Wien, M. (1928). *Phys. Z.* **29**, 751–755.

Wien, M. (1931). *Phys. Z.* **32**, 545–547.
Young, T. F., Maranville, L. F., and Smith, H. M. (1959). *In* "The Structure of Electrolytic Solutions" (W. J. Hamer, ed.), pp. 35–63. Wiley, New York.
Zwanzig, R. W. (1965). *Annu. Rev. Phys. Chem.* **16**, 67–102.
Zwanzig, R. W. (1970). *J. Chem. Phys.* **52**, 3625–3628.